Cervicovaginal tissue residence imprints a distinct differentiation program upon memory CD8 T cells

Veronica Davé[1,2], E. Fabian Cardozo-Ojeda[1], Florian Mair[1], Jami Erickson[1], Amanda S. Woodward-Davis[1], Amanda Koehne[3], Andrew Soerens[1], Julie Czartoski[1], Candice Teague[1], Nicole Potchen[1,2], Susanne Oberle[4], Dietmar Zehn[4,†], Joshua T. Schiffer[1,5,6], Jennifer M. Lund[1,2,*], Martin Prlic[1,2,7*]

[1] Vaccine and Infectious Disease Division, Fred Hutchinson Cancer Research Center, Seattle, WA 98109

[2] Graduate Program in Pathobiology, Department of Global Health, University of Washington, Seattle, WA 98195

[3] Comparative Pathology, Fred Hutchinson Cancer Research Center, Seattle, WA 98109

[4] Division of Immunology and Allergy, Department of Medicine, Lausanne University Hospital, 1011 Lausanne, Switzerland

[5] Clinical Research Division, Fred Hutchinson Cancer Research Center, Seattle, WA 98109

[6] Department of Medicine, University of Washington, Seattle, WA 98195

[7] Department of Immunology, University of Washington, Seattle, WA 98195

[*]Co-corresponding authors (jlund@fredhutch.org, mprlic@fredhutch.org)

[†]Present address: Division of Animal Physiology and Immunology, School of Life Sciences Weihenstephan, Technical University of Munich, 85354 Freising, Germany

Running title: Cervicovaginal CD8 T cell memory

Summary (~40 words)

The tissue-resident memory (T_{RM}) CD8 T cell compartment in human and mouse cervicovaginal tissue (CVT) is remarkably similar. The CVT T_{RM} compartment is maintained autonomously and does not reach phenoypical or numerical equilibrium. The numerical decline leads to impaired viral control in a secondary challenge.

Abstract (160 words)

Tissue-resident memory CD8 T cells (CD8 T_{RM}) are critical for maintaining barrier immunity. CD8 T_{RM} have been mainly studied in the skin and gut with recent studies suggesting that the signals that control tissue-residence and phenotype are highly tissue-dependent. We examined the T cell compartment in healthy human cervicovaginal tissue (CVT) and found that most CD8 T cells were granzyme B^+ and TCF-1^-. To address if this phenotype is driven by CVT tissue-residence, we used a mouse model to control for environmental factors. Using localized and systemic infection models, we found that CD8 T_{RM} in the mouse CVT gradually acquired a granzyme B^+, TCF-1^- phenotype as seen in human CVT. In contrast to CD8 T_{RM} in the gut, these CD8 T_{RM} were not stably maintained regardless of the initial infection route, which led to reductions in local immunity. Our data show that residence in the CVT is sufficient to progressively shape the size and function of its CD8 T_{RM} compartment.

46 **Introduction**

47 After infection or immunization, naive CD8 T cells differentiate into several major
48 populations of memory T cells with distinct functions and trafficking patterns. Tissue-resident
49 memory CD8 T cells (CD8 T_{RM}) are a major subset defined by the fact that they do not
50 recirculate via blood and lymph, instead remaining in the tissue sites where they were initially
51 seeded by effector T cells during the primary response (Gebhardt et al., 2009; Masopust et al.,
52 2010; Masopust and Soerens, 2019; Szabo et al., 2019; Wakim et al., 2008). Because of their
53 privileged location, CD8 T_{RM} are uniquely poised to respond to subsequent encounters with their
54 cognate antigen by directly killing infected cells (Casey et al., 2012; Steinbach et al., 2016),
55 proliferating to boost the local CD8 T cell pool (Beura et al., 2018; Park et al., 2018), and
56 activating and recruiting additional immune cells from both resident and circulating populations
57 (Ariotti et al., 2014; Schenkel et al., 2013).

58 Many factors influence the formation of T_{RM}, including the route of priming, exposure to
59 antigen and inflammation, and the type of tissue in which residency is established. For example,
60 the presence of local antigen boosts the size and function of T_{RM} populations within the matched
61 tissue site (Davies et al., 2017; Gebhardt et al., 2009; Khan et al., 2016; Schenkel et al., 2013).
62 Similarly, local inflammation enhances the number and function of T_{RM} in an antigen-
63 independent manner (Mackay et al., 2012; Shin and Iwasaki, 2012) and cytokine cues such as
64 TGF-β, IL-15, and CCL5 appear to directly regulate T_{RM} formation and maintenance
65 (Bergsbaken et al., 2017; Iijima and Iwasaki, 2014; Mackay et al., 2015; Zhang and Bevan,
66 2013).

67 Despite the importance of local exposure to antigen and inflammation in T_{RM}
68 development, strong evidence also exists that T_{RM} can broadly seed distal tissues after both
69 systemic and local immunization or infection. Systemic immunization and infection models are
70 routinely used in mice to generate T_{RM} populations across many body sites (Masopust et al.,

71 2001; Milner et al., 2017; Pope et al., 2001; Reinhardt et al., 2001; Steinert et al., 2015).
72 Likewise, localized infections such as herpes simplex virus (HSV) and vaccinia virus seed CD8
73 T_{RM} at distal tissue sites, albeit to a much lower extent than at the primary site of infection
74 (Davies et al., 2017; Jiang et al., 2012; Khan et al., 2016; Masopust et al., 2004). Together, these
75 studies suggest that T_{RM} can develop within diverse tissue sites across a range of levels of
76 inflammation and antigen availability, and it is currently unclear how the combination of these
77 variables may ultimately tune the characteristics of the resulting T_{RM} population.
78 The tissue of residence itself also impacts the phenotype of CD8 T_{RM} populations. CD8
79 T_{RM} have been extensively studied in skin of both humans and mice, and it is now well-known
80 that skin-resident CD8 T cells express the putative residency markers CD69 and integrin α_E
81 (CD103), respond to local HSV infection, and rely on TGF-β and IL-15 signals for their
82 development (Gebhardt et al., 2009; Mackay et al., 2013; Watanabe et al., 2015; Zhu et al.,
83 2013). Many reports suggest that CD8 T_{RM} in other organs may differ in their phenotype or
84 developmental requirements. For example, it is well-documented that CD69 and CD103 are not
85 necessarily expressed by T_{RM} in the uterus or pancreas (Steinert et al., 2015) but may be
86 required by T_{RM} in other organs such as the salivary gland, lung, or kidney (Hofmann and
87 Pircher, 2011; Takamura et al., 2016; Walsh et al., 2019). Likewise, some organs such as the
88 small intestine maintain T_{RM} that constitutively express granzyme B in the absence of antigen or
89 re-challenge (Casey et al., 2012; Kim et al., 1997), a phenotype which has not been observed as
90 robustly in other tissue sites, including the lung and uterus (Beura et al., 2019; Piet et al., 2011).
91 It remains an open question whether CD8 T_{RM} phenotype is inextricably linked to tissue of
92 residence, or whether alterations to the priming method or the inflammatory milieu within a
93 tissue could elicit features such as constitutive granzyme B expression in tissue sites where
94 they are not normally observed.

95 Mucosal barrier tissues contain large populations of CD8 T_{RM}, and pathogens that infect
96 mucosal barrier surfaces represent a significant global health burden. Specifically, the study of
97 CD8 T cell memory within the cervicovaginal tissue (CVT) has broad importance in
98 understanding the pathogenesis and vaccinology of sexually-transmitted infections. Compared
99 to memory CD8 T cells in the upper female reproductive tract and other mucosal and lymphoid
100 tissues, the phenotypic and functional characteristics of memory CD8 T cells in the CVT remain
101 relatively understudied. We recently reported that the CD8 T cell compartment in human CVT
102 includes a subset of CD8 T cells that robustly express granzyme B (Pattacini et al., 2019). It is
103 unclear to what extent the distinctive features we observed in human CVT may be driven by
104 recurring local infections, exposure to inflammatory cues, or a result of signals intrinsically
105 associated with the cervicovaginal microenvironment.
106 Here, we report that CD8 T cells isolated from healthy human CVT lacked expression of
107 the memory-associated transcription factor TCF-1 and resembled effector or terminally-
108 differentiated cells rather than a self-renewing memory T cell population. To determine if this
109 characteristic was driven by residence in the tissue itself or was a consequence of local
110 exposure to antigenic insults or inflammation in human CVT, we utilized multiple immunization
111 strategies to assess memory CD8 T cell differentiation and maintenance in the mouse CVT. We
112 found that memory CD8 T cells in the mouse CVT at later memory time points closely
113 resembled the CD8 T cells found in human CVT regardless of the initial immunization route and
114 early phenotypic differences. Memory CD8 T cell numbers where stably maintained in the
115 periphery and gut, but gradually declined in the CVT over five months post-immunization, which
116 was associated with a delay in viral control upon HSV vaginal challenge. We conclude that
117 residence in the CVT is sufficient to alter the canonical differentiation and maintenance program
118 of memory CD8 T cells.
119

120 **Results**

121 *Healthy human cervicovaginal tissue contains CD8 T cells that express granzyme B and lack*
122 *TCF-1*

123 In order to study the phenotypic profile of CD8 T cells within human CVT from healthy
124 women without any genital infections, we isolated lymphocytes from human vaginal biopsies via
125 enzymatic digestion (**Fig. S1A**) and observed that the majority of memory T cells in this tissue
126 site expressed the residency markers CD69 and CD103 (**Fig. 1A-B**). A large proportion of these
127 CD8 T cells expressed granzyme B *ex vivo* (**Fig. 1C**) and the majority of granzyme B^+ cells co-
128 expressed CD103 (**Fig. 1D**), suggesting that they were potentially resident within the tissue
129 rather than transient inflammatory cells. We observed that the memory CD8 T cell compartment
130 in human CVT lacked expression of TCF-1 (**Fig. 1E**), a transcription factor associated with self-
131 renewal potential in CD8 T cells (Zhou et al., 2010). These data indicated that human memory
132 CD8 T cells within the CVT may possess functional and proliferative characteristics distinct from
133 such cells in other tissue locations.

134

135 *Vaginal immunization in mice results in a CD8 T cell compartment that resembles that of human*
136 *CVT*

137 We next wanted to address if this human CVT CD8 T cell phenotype was attributable to
138 ongoing basal levels of antigenic insult or inflammation in the tissue, or might represent more
139 generalized characteristics of CD8 T cells in CVT. To stringently control for external
140 environmental factors, we sought to generate a comparable population of memory CD8 T cells
141 in mouse CVT. We adoptively transferred naive gBT-I CD8 T cells specific to the SSIEFARL
142 epitope from HSV and primed these cells by vaginal infection with non-lethal thymidine-kinase
143 deficient HSV-2 (HSV-2 TK-) (**Fig. 2A**). One month following infection, HSV gB $tetramer^+$ CD8 T
144 cells in the CVT expressed CD69, CD103, and granzyme B in similar proportions to those
145 observed in human CVT (**Fig. 2B-C**). In addition, we found that these CD8 T cells largely lacked

146 expression of TCF-1, especially compared to gB tetramer$^+$ cells in the vaginal-draining lymph
147 nodes (dLN) (**Fig. 2D**). Given that these mice had received a vaginal infection, we wondered if
148 this granzyme B$^+$ TCF-1$^-$ phenotype might be a result of ongoing inflammatory responses in the
149 CVT. Indeed, analysis of hematoxylin and eosin-stained sections of CVT from infected mice
150 revealed that clusters of inflammatory cells remained in the CVT lamina propria as long as 22d
151 after infection (**Fig. 2E**), suggesting that inflammation was not resolved by this time point. Thus,
152 our data suggested that prolonged local tissue inflammation could be driving this distinct
153 memory CD8 T cell phenotype within the CVT.
154
155 *Systemic immunization with LM-gB elicits stable HSV-specific CD8 T cell memory in secondary*
156 *lymphoid organs and the small intestine, but not the CVT*
157 To determine if prolonged tissue inflammation drives this CVT memory T cell phenotype,
158 we used a systemic immunization approach to prime gBT-I cells in the absence of significant
159 vaginal inflammation. We generated a recombinant strain of *Listeria monocytogenes* that
160 expresses the HSV-derived SSIEFARL peptide (LM-gB) and immunized mice intravenously
161 (**Fig. 3A**). We confirmed that this immunization strategy did not result in detectable levels of
162 vaginal inflammation compared to uninfected mice, and caused significantly less inflammation
163 than observed in mice vaginally immunized with HSV-2 TK- (**Fig. 3B)**. In addition, immunized
164 mice mounted a robust systemic HSV-specific CD8 T cell response, with gB-specific T cells
165 making up an average of 36.4% of CD8 T cells in the blood by 1wk after immunization (**Fig. 3C**).
166 At 1mo after immunization, we could identify these cells in multiple body sites including the CVT
167 and vaginal-draining lymph nodes (**Fig. S1B** and **Fig. 3D**). Again, CD103$^+$ gB-specific CD8 T
168 cells in the CVT lacked expression of TCF-1, replicating the phenotype observed in both human
169 vaginal tissue and CVT of vaginally-immunized mice (**Fig. 3E**), despite the lack of tissue
170 inflammation.

171 Given this evidence that memory CD8 T cells in CVT lack significant expression of TCF-
172 1 regardless of immunization route, we next asked whether this memory compartment was
173 deficient in self-renewal and would undergo gradual decay. While the frequency of memory gB-
174 specific CD8 T cells remained relatively stable in the blood following contraction (**Fig. 3F**), and
175 the number of gB-specific CD8 T cells in the spleen, CVT-draining lymph nodes, and small
176 intestine lamina propria (SI LP) beyond 1mo after immunization was stable, this population
177 underwent a threefold loss in number within the CVT, with some mice having very few gB-
178 specific CD8 T cells remaining in the CVT by 5 months post-immunization (**Fig. 3G**).
179 Interestingly, gB-specific T cells in the SI LP also lacked expression of TCF-1 (**Fig. S2A**),
180 suggesting that memory T cells induced by the same immunization may have different
181 requirements for self-renewal.
182
183 *Loss of memory CD8 T cells in the CVT occurs mainly among the CD69$^-$ CD103$^-$ subset*
184 Given that gB-specific CD8 T cells in the CVT continued to decline in number after T cell
185 contraction had concluded in other tissues, we next examined the expression of canonical
186 markers of tissue residency and effector function. To reliably determine what proportion of the
187 gB-specific CD8 T cells in each organ were located within the tissue, we performed
188 intravascular (i.v.) antibody labeling (Galkina et al., 2005) (**Fig. S1C**). We found that an average
189 of 85.6% of the gB-specific CD8 T cells in the CVT were protected from i.v. labeling by 1mo
190 after immunization, similar to the fraction within the small intestine lamina propria (**Fig. 4A**). The
191 proportion of CVT gB-specific CD8 T cells that were protected from i.v. labeling remained stable
192 across time points, suggesting that the smaller population of T cells remaining at late time points
193 continued to be composed of cells that were mostly located within the tissue parenchyma (**Fig.
194 4A**).
195 We next assessed whether gB-specific CD8 T cells expressed CD69 and CD103. We
196 found that these markers were mostly non-expressed on gB-specific CD8 T cells at the earliest

197 memory time point. However, the average frequency of CD103$^+$ cells within the gB-specific CD8
198 T cell subset increased from 20.6% to 54.4% between 1mo and 5mo after LM-gB immunization
199 (**Fig. 4B-D**). While the i.v.-label$^+$ fraction of gB-specific CD8 T cells in the CVT remained almost
200 completely CD103$^-$ for the entire duration of the experiment, the shift from a predominantly
201 CD103$^-$ population to a predominantly CD103$^+$ population was especially clear within the i.v.-
202 label$^-$ fraction of CVT gB-specific CD8 T cells (**Fig. 4C-D**) and was mainly attributable to a
203 relative loss of CD103$^-$ cells from the CVT over time (**Fig. 4E**). Conversely, the equivalent i.v.
204 label$^-$ fraction of gB-specific CD8 T cells in the SI LP, did not undergo a population-level shift
205 towards becoming CD103$^+$ (**Fig. 4C**). Finally, the total CD69$^+$ CD103$^+$ population in the CVT
206 was stably maintained over time (**Fig. 4E**), which could be due to conversion of other subsets to
207 a CD69$^+$ CD103$^+$ phenotype or the ability to self-renew at a rate sufficient for stable
208 maintenance.
209
210 *CVT memory CD8 T cells induced by systemic immunization gradually acquire expression of*
211 *granzyme B*
212 We next wanted to determine if systemic immunization resulted in constitutive granzyme
213 B expression by CD8 T cells in the CVT, as we observed after vaginal immunization (**Fig. 2**) and
214 as described for tissue-resident CD8 T cells in the SI LP, which express granzyme B in the
215 absence of antigen re-exposure (Casey et al., 2012; Masopust et al., 2006). Few gB-specific
216 CD8 T cells in the CVT expressed granzyme B at 1mo after LM-gB immunization, but the
217 granzyme B$^+$ population substantially increased in both number and frequency at later time
218 points (**Fig. 5A-B**). In contrast, a subset of SI LP gB-specific CD8 T cells expressed granzyme B
219 by 1mo after immunization, and expression remained stable thereafter (**Fig. 5A**). As expected,
220 granzyme B expression was rarely observed among gB-specific CD8 T cells in the spleen or
221 dLN, regardless of the memory timepoint (**Fig. 5A**).

222 We next examined the phenotypic identity of these granzyme B-expressing cells. By
223 3mo post-immunization, granzyme B^+ gB-specific CD8 T cells in the CVT were almost
224 exclusively $CD103^+$ (**Fig. 5C-E**), resembling our results in human samples (**Fig. 1D**) and
225 suggesting that these two dynamically-expressed markers were demarcating the same cellular
226 population. By contrast, the granzyme B^+ population in the SI LP comprised both $CD103^+$ and
227 $CD103^-$ cells (**Fig. 5D-E**). These data suggest that immunization-induced gB-specific memory
228 CD8 T cells differentiate asynchronously in the CVT relative to the gut mucosa or peripheral
229 lymphoid organs.
230
231 *Numeric and phenotypic changes of HSV-specific memory T cells in the CVT lead to delayed*
232 *protection against viral challenge.*
233 Given the decline in the number of gB-specific CD8 T cells in the CVT combined with
234 their shift towards CD103 and granzyme B expression, we next evaluated how these changes
235 affected the immunoprotective response to vaginal HSV-2 challenge. Because LM-gB does not
236 prime HSV-specific CD4 T or B cells responses, this immunization system allowed us to
237 specifically assess the protective effect of CD8 T cells in the absence of other antigen-specific
238 responses. We presumed that the most rapid antiviral responses would likely be mediated by
239 tissue-resident gB-specific CD8 T cells, while circulating gB-specific CD8 T cells would
240 contribute to later responses. We challenged immunized mice at either 1mo ("Early Memory") or
241 4mo ("Late Memory") after immunization (**Fig. 6A**). A similar proportion of mice in each group
242 survived lethal challenge (**Fig. 6B**), demonstrating that gB-specific memory CD8 T cells were
243 sufficient to confer protection against HSV-2 lethality in a subset of immunized mice. However,
244 mice challenged earlier after immunization began to show evidence of faster viral clearance
245 starting as early as 3.5d after challenge (**Fig. 6C**) and underwent greater T cell expansion in the
246 first 2.5d after challenge (**Fig. 6D**). We hypothesized that this was due to quantitative and
247 qualitative differences between the early and late CD8 T cell compartment in the CVT.

248 To better understand the relationship between CVT gB-specific CD8 T cells and viral
249 control, we built upon our previously described approaches to model the acute T cell response
250 to HSV-2 infection (Schiffer et al., 2010; Schiffer et al., 2013) and used the mathematical model
251 in **Equation 1** to characterize the different gB-specific T cell response kinetics between the
252 early and late memory groups. In this model, susceptible cells in the CVT are infected by free
253 HSV-2, allowing them to produce new virus or be killed by HSV-specific CD8 T cells (**Fig. 6E**).
254 We performed 100 model-fit rounds to all observations simultaneously for each group for
255 experimentally-determined CVT gB-specific CD8 T cell counts and viral load and overlaid these
256 predictions onto our experimental data (**Fig. 6D)**. In naive mice, gB-specific CD8 T cells were
257 absent from or rare in the CVT at 0-3.5d after challenge but were abundant by 6.5d after
258 challenge (**Fig. 6D**, top left), corresponding with the entry of effector T cells into the CVT
259 following primary infection. In mice challenged at either early or late time points, gB-specific
260 CD8 T cells increased dramatically in number between 0d and 2.5d after HSV-2 infection, and
261 HSV viral titer fell by 6.5 post-challenge (**Fig. 6D**). The best model fits predicted that naive mice
262 had the highest basic reproductive number, meaning that they had the highest number of new
263 cellular infections predicted to derive from a single HSV-infected cell in a susceptible pool (**Fig.**
264 **6F**). In addition, the greater areas under fitted gB tet$^+$ T cell curves (shown in **Fig. 6D**, top row)
265 were associated with earlier viral clearance (**Fig. 6G**). These data suggest that the numeric and
266 phenotypic changes we observed within the CVT memory T cell compartment led to a decrease
267 in the efficacy of the anti-viral response in the first days after challenge.
268
269 *Progressive differentiation by the memory CD8 T cell compartment in the CVT does not require*
270 *new input of cells from circulation*
271 To determine if the CVT-specific changes in the memory T cell compartment occurred in
272 a tissue-autonomous manner, we depleted Thy1.1$^+$ gBT-I cells from the blood and lymphoid
273 tissues of LM-gB immunized mice 1mo after immunization (**Fig. 7A)**, as previously described

274 (Schenkel et al., 2013). This method depleted splenic and circulating gBT-I cells but left the CVT
275 gBT-I compartment intact (**Fig. 7B-C**) and did not have a major impact on protection against
276 vaginal challenge with HSV-2 (**Fig. S3A-B**). By 3mo after depletion, we observed that a similar
277 level of decay had occurred among the CVT gB-specific CD8 T cell population to that seen in
278 undepleted mice between 1mo and 5mo after immunization (**Figs. 3G and 7C**). Similar to our
279 previous results, we observed that this decay occurred mostly among the CD103$^-$ subset of T
280 cells (**Fig. 7D-E**) and that the persisting cells had upregulated granzyme B by 3mo after
281 immunization (**Fig. 7F**). Low TCF-1 expression remained stable from 1mo to 3mo after
282 immunization but was reduced by gBT-I depletion, suggesting that the small TCF-1$^+$ subset in
283 the CVT of immunized mice was partially but not completely attributable to recirculating gBT-I
284 cells (**Fig. 7G**). These data indicate that the granzyme B$^+$ subset of gB-specific cells stems from
285 granzyme B$^-$ cells that were present in the tissue 1mo after immunization.
286
287 *The memory CD8 T cell compartment in the CVT undergoes numeric decay regardless of*
288 *priming infection and immunization route*
289 Finally, we wished to determine whether site-matched immunization would result in
290 improved maintenance of the CVT memory CD8 T cell compartment. We compared the
291 maintenance of HSV-specific CD8 T cells in the CVT of mice immunized vaginally with HSV-2
292 TK- or intravenously with LM-gB (**Fig. 8A**). We observed that vaginal immunization with HSV-2
293 TK- did not result in a larger memory population of HSV-specific CD8 T cells in the CVT than
294 systemic immunization with LM-gB (**Fig. 8B**). In addition, the gB-specific population induced by
295 vaginal immunization was relatively stably maintained in the spleen and SI LP, but underwent
296 decay in the CVT between 1mo and 3mo after immunization (**Fig. 8B**). Despite this decay in the
297 CD8 T cell compartment, HSV-2 TK- immunized mice remained completely protected against

298 lethal vaginal challenge with wildtype HSV-2 (**Fig. S3**), presumably due to CD4 T cells providing

299 substantial protection in this model (Milligan et al., 1998).

300

301 **Discussion**

302 Here, we report that CVT microenvironment plays a dynamic role in shaping the
303 numeric, phenotypic, and functional characteristics of the tissue memory CD8 T cells, which
304 thereby impacts their immunoprotective potential. The cervicovaginal mucosa is distinct from
305 other parts of the female reproductive tract and other mucosal tissues in terms of epithelium
306 type and physiology. Specifically, the vagina and ectocervix are composed of type II mucosa
307 and the endocervix and uterus are composed of type I mucosa, with the cervical transformation
308 zone marking the area where the simple columnar epithelial cells of the endocervix meet the
309 stratified squamous epithelial cells of the ectocervix and vagina. In contrast, the gut and the
310 lung, other mucosal tissues commonly studied in the case of CD8 T cell memory, are type I
311 mucosal surfaces (Iwasaki, 2010). In addition to these differences in the structure of the
312 epithelium, there are differences in the complexity and makeup of the microbiota at different
313 mucosal tissue sites (Anahtar et al., 2018), which may also contribute to tissue-specific
314 environmental differences that could affect memory CD8 T cell differentiation and function.
315 Vaginal-resident CD8 T cells in healthy women did not express TCF-1 (**Fig. 1**), which could
316 either simply indicate recent activation of these T cells (recent infection) or a memory population
317 with an impaired ability to self-renew. Importantly, given that vaginal CD8 T cells from multiple
318 donors uniformly lacked TCF-1 expression, it suggested that a tissue-driven phenotype was
319 more likely than a recent infection in a cohort of healthy donors with no current genital
320 infections. Using a mouse model, we similarly found that both vaginal (**Fig. 2**) and systemic
321 (**Fig. 3**) immunization resulted in a TCF-1^{low} phenotype among CD8 T cells in the mouse CVT.
322 These data demonstrate that the mouse and human memory CD8 T cell phenotype are
323 remarkably well conserved in the CVT.
324

325 Over the course of 5 months following immunization, antigen-specific memory CD8 T
326 cells in the CVT numerically declined and gradually acquired expression of CD103 and
327 granzyme B. Conversely, HSV-specific CD8 T cells that were circulating (spleen, LN) or resident
328 in the small intestine were numerically and phenotypically stable over the same time course.
329 This decline in CVT T_{RM} memory occurred at a similar rate even when the circulating gBT-I T
330 cells were selectively depleted, suggesting that peripheral T cells do not reseed the CVT under
331 homeostatic conditions (**Fig. 7**). In addition, the CVT CD8 T cell compartment upregulated
332 granzyme B in the absence of new input from the periphery, supporting the occurrence of
333 tissue-intrinsic memory differentiation. Thus, our data show that memory CD8 T cell
334 maintenance and differentiation in the CVT is ultimately directly and uniquely regulated by the
335 tissue environment. A possible explanation for these differences between the vagina and other
336 mucosal tissues such as the gut is that the CVT tissue microenvironment is lacking signals that
337 are important for resident-memory formation and maintenance (Liu et al., 2018). It is noteworthy
338 that we did not observe strong TCF-1 expression in the gut T_{RM} cells either, but these cells were
339 stably maintained over time. This could either suggest that TCF-1 is not required for self-
340 renewal of T_{RM}, or the existence of other compensatory mechanisms to maintain the T_{RM}
341 compartment in certain mucosal tissues. TCF-1 activity is thought to be regulated by β-catenin
342 and the Wnt signaling pathway. However, β-catenin does not regulate the phenotype of memory
343 T cells (Driessens et al., 2010) and β-catenin-deficient T cells mount normal recall responses
344 (Prlic and Bevan, 2011). Since β-catenin is sufficient, but not necessary to activate TCF-1
345 (Tiemessen et al., 2014), a β-catenin-independent pathway may control TCF-1 activity in tertiary
346 tissues with distinct cell fate outcomes compared to β-catenin-dependent activation. A recent
347 study provides some genetic evidence that TCF-1 negatively regulates CD103 expression in the
348 lung tissue (Wu et al., 2020), indicating the need to further study and dissect the role of TCF-1
349 in controlling differentiation and maintenance of T_{RM} cells.

350 Understanding the relationship between T_{RM} in mucosal tissues and the periphery is
351 highly relevant, because memory T cell characteristics and frequencies in the blood are used as
352 a benchmark in clinical studies to assess immune responses to vaccines and to establish
353 correlates of protection (Koup et al., 2011; Lewinsohn et al., 2017; Stephenson et al., 2016;
354 Streeck, 2016). Our data indicate that there is a disconnect between memory CD8 T cell
355 frequency, phenotype, and stability in the periphery and the CVT. The numerical and
356 phenotypical changes of the memory CD8 T cell compartment one month vs. 5 months post-
357 immunization ultimately influenced the rapidity of the immune response to vaginal viral
358 challenge (**Fig. 6**). This may be of particular relevance to the success of a vaccine-induced
359 memory T cell response within the CVT, as the host-pathogen events occurring within this early
360 window likely result in the ultimate success or failure of the protective response (Haase, 2010).
361 Barrier immunity in the CVT remains poorly understood, but is of particular interest,
362 because sexually-transmitted infections (STI) have a significant impact on global health. We
363 currently lack effective vaccines to prevent the majority of these infections, including HIV, HSV,
364 and bacterial STIs. Our data demonstrate that following systemic immunization, animals were
365 partially protected against HSV-2 lethality by gB-specific memory CD8 T cells (**Fig. 6**).
366 Importantly, this protective effect was observed despite the lack of HSV-specific CD4 T or B cell
367 memory, elements of the immune response that are often considered crucial for protection
368 against HSV-2 (Dudley et al., 2000; Milligan et al., 1998; Morrison et al., 1998; Petro et al.,
369 2016). In line with this observation, results from participants with recurrent genital HSV-2
370 infection indeed suggest that CD8 T cell activity within lesions is associated with viral control
371 (Peng et al., 2012; Schiffer et al., 2010; Zhu et al., 2007; Zhu et al., 2013). It is possible that a
372 new focus on vaccine strategies that elicit memory CD8 T cells within the genital mucosa, the
373 site of first exposure to STIs, will increase vaccine efficacy. However, successful design of these
374 approaches, not just in regards to adjuvant and immunization route, but also boosting intervals

375 to optimize protection, relies on understanding how memory CD8 T cells are maintained within
376 these genital tract mucosal tissues.
377 In summary, we demonstrate that the CVT tissue environment controls memory CD8 T
378 cell differentiation and maintenance, which occurs in a tissue autonomous manner and differs
379 across mucosal tissue compartments. The CD8 T_{RM} compartment in the CVT declines over time
380 with a concomitant decrease in the ability to mediate rapid antigen-specific protection.
381

382 **Methods**

383 *Mice*

384 C57BL/6J and B6.PL-*Thy1*^{a}/CyJ mice were purchased from The Jackson Laboratory and
385 maintained in specific pathogen-free conditions at the Fred Hutchinson Cancer Research
386 Center (FHCRC). All mice used in experiments were female and were 8–12 weeks of age. Mice
387 that rejected transferred Thy1.1^{+} gBT-I cells or had an undetectable HSV-2 titer in vaginal wash
388 at 2.5d post-challenge were excluded from experiments. Experiments were approved by the
389 FHCRC Institutional Animal Care and Use Committee.

390

391 *Study population*

392 Women recruited for this study (n=13) consented to vaginal biopsy and blood sampling.
393 Eligibility criteria included aged > 18 to < 45, assigned female sex at birth, in good general
394 health, normal PAP smear within the past 3-5 years, not menopausal, Hepatitis C negative and
395 no report of active genital tract irritation or infection. Additionally, participants were screened to
396 be negative for HIV, HSV-2, bacterial vaginosis, chlamydia, gonorrhea, and trichomonas
397 vaginalis. Subjects were not using any type of steroid or medication for treatment of
398 autoimmune disorders. Samples were not collected during menses. Informed written consent
399 was obtained from all participants. The study and procedures were approved by the FHCRC
400 Institutional Review Board.

401

402 *Adoptive CD8 T cell transfers*

403 CD44^{low} CD8 T cells were purified via negative selection from spleen and lymph nodes
404 using mouse CD8a^{+} T Cell Isolation kits (Miltenyi) as previously described (Prlic et al., 2001). 5
405 × 10^{4} cells were injected into recipient B6 mice via i.v. injection into the tail vein.

406

407 *Herpes simplex virus type 2 infections and quantification*

408 Mice were injected subcutaneously with 2 mg of medroxyprogesterone acetate injectable
409 suspension (Greenstone). Seven days later, mice were infected intravaginally with 2×10^4 pfu
410 wildtype HSV-2 (strain 186 syn+) or 1.88×10^5 PFU of thymidine kinase-negative HSV-2 186
411 kpn to the vaginal canal in a 10 ul volume (Parr et al., 1994). After infection with wildtype HSV-2,
412 mice were monitored daily and clinical disease progression was scored as follows: 0, No sign; 1,
413 slight genital erythema; 2, moderate genital erythema and edema; 3, significant genital
414 inflammation with visible lesion; 4, hind leg paralysis or other severe condition requiring
415 euthanasia; 5, moribund or dead. Mice were euthanized if they were moribund or showed signs
416 of severe disease, including hind leg weakness, hind leg paralysis, or hunched posture. Viral
417 titer was determined by plaque assay on Vero cells (ATCC) or by PCR as previously described
418 (Jerome et al., 2002).
419
420 *Listeria monocytogenes immunization*
421 A strain of *Listeria monocytogenes* (LM) was generated to recombinantly express and
422 secrete ovalbumin containing the HSV-2 glycoprotein B-derived peptide SSIEFARL according to
423 previously described methods (Lauer et al., 2002; Zehn et al., 2009). Stocks were diluted to $2 \times$
424 10^4 CFU per ml in sterile PBS before immunization. Naive B6 mice received 4,000 CFU i.v. via
425 tail vein injection. Infectious dose was confirmed by plating on brain-heart infusion media plates
426 and enumerating colonies.
427
428 *Labeling of T cells in the vasculature*
429 To discriminate CD8 T cells in the vasculature from those located within tissues, we
430 utilized an intravascular labeling technique as previously described (Galkina et al., 2005).
431 Briefly, mice were injected i.v. with 3 ug anti-CD8b antibody conjugated to either FITC or APC

432 (Clone: H35-17.2, eBioscience) in PBS via the tail vein 2-5 min before euthanasia by CO_2
433 inhalation.
434
435 *Depletion of Thy1.1-expressing T cells*
436 Mice were injected intraperitoneally with 500 ng anti-Thy1.1 antibody (Clone 19E12, Bio
437 X Cell) to deplete Thy1.1-expressing cells from the circulation and peripheral lymphoid tissues.
438
439 *Tissue collection and processing*
440 Mouse
441 For pathologic assessment, murine cervicovaginal tracts (consisting of the vagina,
442 ectocervix, and endocervix) were fixed in 10% formalin, embedded in paraffin, sectioned, and
443 stained with hematoxylin and eosin.
444 To prepare single cell suspensions, cervicovaginal tracts were minced with scissors and
445 then incubated in 2 ml DMEM medium supplemented with 2% FBS, 2 mg/ml collagenase D
446 (Roche), and 1.5 mg/ml DNase I (Roche) for 30 minutes at 37C with gentle rocking. Single cell
447 suspensions were prepared from small intestines by removing the Peyer's patches and
448 mesentery, incubated in HBSS with 2% FBS, 5 mM EDTA, and 1 mM dithiothreitol for 15 min at
449 37C with gentle rocking, followed by collagenase treatment as outlined for the CVT.
450
451 Human
452 Blood was collected into acid citrate dextrose tubes. Tissues were transported from the clinic in
453 ice cold PBS and immediately processed upon arrival. Biopsy samples were trimmed to $2mm^2$
454 pieces and digested with collagenase II (700 units/ml, Sigma-Aldrich) and DNAse I (1unit/ml,
455 Sigma-Aldrich) for two subsequent 30 minute-digestions at 37°C as previously described
456 (McKinnon et al., 2014). Single cell suspensions were then washed and filtered before use.

457

458 *Pathologic assessment of mouse vaginal tissue*

459 Hematoxylin and eosin-stained sections of mouse CVT were scored based on signs of
460 inflammation within the vaginal lamina propria as follows: 1, Rare neutrophils and other
461 leukocytes present in the lamina propria; 2, Small clusters of neutrophils and other leukocytes
462 present in the lamina propria; 3, Multifocal clusters of leukocytes beginning to coalesce and/or
463 form follicles within the lamina propria; 4, Leukocytes arranged in sheets within the lamina
464 propria. Scoring was performed by a veterinary pathologist who was blinded to group identities.

465

466 *Cell Staining for Flow Cytometry and Sorting*

467 Cells were incubated in LIVE/DEAD fixable amine-reactive viability dye (Invitrogen),
468 blocked for Fc binding (Clone 2.4G2 for mice or TruStain (BioLegend) for human), and then
469 stained with tetramers and antibodies.

470 The following fluorochrome-conjugated antibodies were used to stain mouse cells for
471 flow cytometry: anti-CD8 (Clone 53-6.7, PerCP-eFluor710), anti-CD4 (Clone GK1.5, APC-
472 eFluor780), anti-CD45.1 (Clone A20, Brilliant Ultraviolet 395), anti-CD45.2 (Clone 104, Brilliant
473 Ultraviolet 737), anti-Thy1.1 (Clone HIS51, FITC or SuperBright645), anti-CD44 (Clone IM7,
474 APC or AlexaFluor700), anti-CD69 (Clone H1.2F3, PE-Dazzle594 or PE-Cy7), anti-CD103
475 (Clone M290, Brilliant Violet 786), anti-granzyme B (Clone GB11, Pacific Blue), and anti-TCF-1
476 (Clone C63D9, PE). Anti-CD8, anti-CD4, and anti-Thy1.1 were purchased from eBioscience.
477 Anti-CD45.1, anti-CD45.2, anti-CD44, and anti-CD103 were purchased from BD. Anti-CD69 and
478 anti-granzyme B antibodies were purchased from Biolegend. Anti-TCF-1 antibody was
479 purchased from Cell Signaling Technologies.

480 The following fluorochrome-conjugated antibodies were used to stain human cells for
481 flow cytometry: anti-CD3 (Clone UCHT1, Brilliant Ultraviolet 661), anti-CD45 (Clone HI30,
482 Brilliant Ultraviolet 805), anti-CD8 (Clone RPA-T8, Brilliant Ultraviolet 496), anti-CD4 (Clone

483 RPA-T4, Brilliant Violet 605), anti-CD45RA (Clone HI100, APC-H7), anti-CCR7 (Clone G043H7,
484 AlexaFluor488), anti-granzyme B (Clone GB11, AlexaFluor700), anti-CD103 (Clone Ber-ACT8,
485 Brilliant Violet 750), and anti-TCF-1 (Clone C63D9, PE). Anti-CD3, anti-CD45, anti-CD4, anti-
486 CD8, anti-CD45RA, anti-CD103, and anti-granzyme B were purchased from BD. Anti-CCR7
487 antibody was purchased from Biolegend. Anti-TCF-1 antibody was purchased from Cell
488 Signaling Technologies.
489 Intracellular staining was conducted after fixation and membrane permeabilization using
490 Cytofix/Cytoperm Fixation/Permeabilization Kits (BD). If TCF-1 was included in the staining
491 panel, intracellular staining was conducted after nuclear permeabilization using
492 Foxp3/Transcription Factor Staining Kits (eBioscience) according to the manufacturer's protocol.
493 Samples were acquired on a FACSymphony instrument (BD) or sorted on a FACSAria (BD). To
494 estimate cell counts, 2×10^5 AccuCheck Counting Beads (ThermoFisher) were added to each
495 sample immediately before acquisition.
496
497 *Statistical Analysis*
498 Sample means between two unpaired groups were compared by *t*-test. Sample means
499 between three or more unpaired groups were compared by ordinary one-way ANOVA with
500 Tukey's multiple comparisons test. Sample means between three paired groups were compared
501 by repeated measures ANOVA with Greenhouse-Geisser correction. Paired mean fluorescence
502 intensity or relative frequency data were analyzed via paired *t*-test. All cell count and viral titer
503 data were $\log_{10}$-transformed before graphing and analysis. Error bars represent standard
504 deviations. Exact *P*-values are given for all results where $P < 0.05$. Analysis was performed
505 using Prism 7 (GraphPad Software).
506
507 *HSV-2 and CD8 T cell Dynamics Modeling*

To understand the virus and gB-specific CD8 T cell dynamic differences between the Naive, Early Memory, and Late Memory groups, we used an acute viral infection model that included a cytotoxic effect of the CD8 T cell compartment. In this model, susceptible cells (S) are infected at rate βVS by free HSV-2 virus (V). Productively HSV-2-infected cells (I) have a clearance that is intrinsic or mediated by a humoral response with rate $\delta_I I$ or a clearance mediated by HSV-specific CD8 T cells (E) with killing rate kEI. Free virus is produced at a rate pI and cleared at rate cV. HSV-specific CD8 T cells are cleared at rate $\delta_E E$ and proliferate in the presence of infected cells at a maximum rate ωEI. We also assumed the proliferation of HSV-specific CD8 T cells is constrained when infected and effector cells grow over saturation levels I_{50} and E_{50}, respectively. Under these assumptions the model has the form (see schematics in **Fig. 6D**):

$$\begin{aligned}
\frac{dS}{dt} &= -\beta VS \\
\frac{dI}{dt} &= \beta VS - \delta_I I - kEI \\
\frac{dV}{dt} &= pI - cV \\
\frac{dE}{dt} &= \frac{\omega EI}{\left(1+\frac{I}{I_{50}}\right)\left(1+\frac{E}{E_{50}}\right)} - \delta_E E.
\end{aligned} \qquad \textbf{(Equation 1)}$$

The basic reproductive ratio, R_0, which represents the number of secondary infections produced by an HSV-infected cell when introduced into a susceptible population, was calculated as $R_0 = \frac{\beta p T_0}{c(\delta_I + kE_0)}$. When $R_0 < 1$, viremia is controlled.

We performed 100 rounds of model fits to observations from all individual animals for each group with different initial parameter guesses in the optimization algorithm. We assumed that all outcomes from the 100 fit rounds were plausible predictions of the data and represented the variability in the infection dynamics in each group. For each round, we re-parameterized the model in function of R_0, and used a nonlinear least-squares approach using the differential evolution and the L-BFGS-B algorithms in R (R Development Core Team) to fit the model and to estimate parameters: V_0, pT_0, E_0, R_0, δ, c, k, ω, δ_E, I_{50} and E_{50}. Since mice were inoculated

530 with ~2.3×10^6 HSV genomes, we set that number as the upper limit for V_0. We also constrained
531 the value estimate E_0 to the maximum and minimum HSV-specific CD8 T cell observations at
532 the moment of virus challenge. Finally, we ensured that $R_0 > 1$ in all fitting rounds. In all
533 simulations $t = 0$ represented the time of the HSV-2 vaginal challenge. From the best fits, we
534 computed the predicted time of viral clearance as the time when viral load crossed the detection
535 limit for the PCR assay of 4615.4 genomes per vaginal wash. We also computed the predicted
536 area under the curve of HSV-specific CD8 T cells using best fits of variable *E* from challenge
537 until the time of viral clearance.

538 We repeated the fits by exploring different possibilities for constraining HSV-specific
539 CD8 T cell growth. Specifically, we explored a model were CD8 growth is constrained only by a
540 saturation level in HSV-infected cells, i.e. $\frac{dE}{dt} = \frac{\omega EI}{\left(1+\frac{I}{I_{50}}\right)} - \delta_E E$, or only by a saturation for the
541 number of effector cells, i.e. $\frac{dE}{dt} = \frac{\omega EI}{\left(1+\frac{E}{E_{50}}\right)} - \delta_E E$. To determine the best and most parsimonious
542 model, we computed the Akaike Information Criteria, $AIC = n \ln \overline{SSE} + 2m$, where *m* is the
543 number of parameters estimated, *n* the number of data points in each group and $\overline{SSE}$ is the
544 average sum of squares error of all the 100 model-fit rounds in each group. We assumed a
545 model had similar support from the data if the difference between its AIC and the best model
546 (lowest) AIC was less than two. We selected and showed results from the model with the lowest
547 AIC.
548

549 **Abbreviations**

550 AIC, Akaike information criteria
551 AUC, area under curve
552 CVT, cervicovaginal tissue
553 dLN, CVT-draining lymph nodes

554 gB, HSV glycoprotein B

555 HSV-2 TK-, thymidine kinase-deficient herpes simplex virus type 2

556 LM-gB, *Listeria monocytogenes* strain expressing the SSIEFARL peptide from HSV glycoprotein

557 B

558 LN, lymph node

559 SI, small intestine

560 SI LP, small intestine lamina propria

561 STI, sexually-transmitted infection

562 **Acknowledgements**

563 We thank Kristin Weakly for excellent technical assistance and Sean M. Hughes for assistance
564 with statistical analyses. This work was supported by NIH grants R01 AI123323 (MP), R01
565 AI121129 to (JTS, JML and MP), R01 AI131914 (JML), R01 AI141435 (JML), T32 AI07140 and
566 the Doug and Maggie Walker Fellowship (ASWD), and T32 AI007509 and F31 AI140514 (VD).
567 FM is an ISAC scholar.

568

569 **References**

570 Anahtar, M.N., D.B. Gootenberg, C.M. Mitchell, and D.S. Kwon. 2018. Cervicovaginal
571 Microbiota and Reproductive Health: The Virtue of Simplicity. *Cell Host Microbe* 23:159-
572 168.

573 Ariotti, S., M.A. Hogenbirk, F.E. Dijkgraaf, L.L. Visser, M.E. Hoekstra, J.Y. Song, H. Jacobs, J.B.
574 Haanen, and T.N. Schumacher. 2014. T cell memory. Skin-resident memory CD8(+) T
575 cells trigger a state of tissue-wide pathogen alert. *Science* 346:101-105.

576 Bergsbaken, T., M.J. Bevan, and P.J. Fink. 2017. Local Inflammatory Cues Regulate
577 Differentiation and Persistence of CD8(+) Tissue-Resident Memory T Cells. *Cell Rep*
578 19:114-124.

579 Beura, L.K., N.J. Fares-Frederickson, E.M. Steinert, M.C. Scott, E.A. Thompson, K.A. Fraser,
580 J.M. Schenkel, V. Vezys, and D. Masopust. 2019. CD4(+) resident memory T cells
581 dominate immunosurveillance and orchestrate local recall responses. *J Exp Med*
582 216:1214-1229.

583 Beura, L.K., J.S. Mitchell, E.A. Thompson, J.M. Schenkel, J. Mohammed, S. Wijeyesinghe, R.
584 Fonseca, B.J. Burbach, H.D. Hickman, V. Vezys, B.T. Fife, and D. Masopust. 2018.
585 Intravital mucosal imaging of CD8(+) resident memory T cells shows tissue-autonomous
586 recall responses that amplify secondary memory. *Nature immunology* 19:173-182.

587 Casey, K.A., K.A. Fraser, J.M. Schenkel, A. Moran, M.C. Abt, L.K. Beura, P.J. Lucas, D. Artis,
588 E.J. Wherry, K. Hogquist, V. Vezys, and D. Masopust. 2012. Antigen-independent
589 differentiation and maintenance of effector-like resident memory T cells in tissues.
590 *Journal of immunology (Baltimore, Md. : 1950)* 188:4866-4875.

591 Davies, B., J.E. Prier, C.M. Jones, T. Gebhardt, F.R. Carbone, and L.K. Mackay. 2017. Cutting
592 Edge: Tissue-Resident Memory T Cells Generated by Multiple Immunizations or
593 Localized Deposition Provide Enhanced Immunity. *Journal of immunology (Baltimore,*
594 *Md. : 1950)* 198:2233-2237.

595 Driessens, G., Y. Zheng, and T.F. Gajewski. 2010. Beta-catenin does not regulate memory T
596 cell phenotype. *Nat Med* 16:513-514; author reply 514-515.
597 Dudley, K.L., N. Bourne, and G.N. Milligan. 2000. Immune protection against HSV-2 in B-cell-
598 deficient mice. *Virology* 270:454-463.
599 Galkina, E., J. Thatte, V. Dabak, M.B. Williams, K. Ley, and T.J. Braciale. 2005. Preferential
600 migration of effector CD8+ T cells into the interstitium of the normal lung. *J Clin Invest*
601 115:3473-3483.
602 Gebhardt, T., L.M. Wakim, L. Eidsmo, P.C. Reading, W.R. Heath, and F.R. Carbone. 2009.
603 Memory T cells in nonlymphoid tissue that provide enhanced local immunity during
604 infection with herpes simplex virus. *Nature immunology* 10:524-530.
605 Haase, A.T. 2010. Targeting early infection to prevent HIV-1 mucosal transmission. *Nature*
606 464:217-223.
607 Hofmann, M., and H. Pircher. 2011. E-cadherin promotes accumulation of a unique memory
608 CD8 T-cell population in murine salivary glands. *Proceedings of the National Academy*
609 *of Sciences of the United States of America* 108:16741-16746.
610 Iijima, N., and A. Iwasaki. 2014. T cell memory. A local macrophage chemokine network
611 sustains protective tissue-resident memory CD4 T cells. *Science* 346:93-98.
612 Iwasaki, A. 2010. Antiviral immune responses in the genital tract: clues for vaccines. *Nat Rev*
613 *Immunol* 10:699-711.
614 Jerome, K.R., M.L. Huang, A. Wald, S. Selke, and L. Corey. 2002. Quantitative stability of DNA
615 after extended storage of clinical specimens as determined by real-time PCR. *J Clin*
616 *Microbiol* 40:2609-2611.
617 Jiang, X., R.A. Clark, L. Liu, A.J. Wagers, R.C. Fuhlbrigge, and T.S. Kupper. 2012. Skin
618 infection generates non-migratory memory CD8+ T(RM) cells providing global skin
619 immunity. *Nature* 483:227-231.

620 Khan, T.N., J.L. Mooster, A.M. Kilgore, J.F. Osborn, and J.C. Nolz. 2016. Local antigen in
621 nonlymphoid tissue promotes resident memory CD8+ T cell formation during viral
622 infection. *J Exp Med* 213:951-966.
623 Kim, S.K., D.S. Reed, W.R. Heath, F. Carbone, and L. Lefrancois. 1997. Activation and
624 migration of CD8 T cells in the intestinal mucosa. *Journal of immunology (Baltimore, Md.*
625 *: 1950)* 159:4295-4306.
626 Koup, R.A., B.S. Graham, and D.C. Douek. 2011. The quest for a T cell-based immune
627 correlate of protection against HIV: a story of trials and errors. *Nat Rev Immunol* 11:65-
628 70.
629 Lauer, P., M.Y. Chow, M.J. Loessner, D.A. Portnoy, and R. Calendar. 2002. Construction,
630 characterization, and use of two Listeria monocytogenes site-specific phage integration
631 vectors. *Journal of bacteriology* 184:4177-4186.
632 Lewinsohn, D.A., D.M. Lewinsohn, and T.J. Scriba. 2017. Polyfunctional CD4(+) T Cells As
633 Targets for Tuberculosis Vaccination. *Front Immunol* 8:1262.
634 Liu, Y., C. Ma, and N. Zhang. 2018. Tissue-Specific Control of Tissue-Resident Memory T Cells.
635 *Crit Rev Immunol* 38:79-103.
636 Mackay, L.K., A. Rahimpour, J.Z. Ma, N. Collins, A.T. Stock, M.L. Hafon, J. Vega-Ramos, P.
637 Lauzurica, S.N. Mueller, T. Stefanovic, D.C. Tscharke, W.R. Heath, M. Inouye, F.R.
638 Carbone, and T. Gebhardt. 2013. The developmental pathway for CD103(+)CD8+
639 tissue-resident memory T cells of skin. *Nature immunology* 14:1294-1301.
640 Mackay, L.K., A.T. Stock, J.Z. Ma, C.M. Jones, S.J. Kent, S.N. Mueller, W.R. Heath, F.R.
641 Carbone, and T. Gebhardt. 2012. Long-lived epithelial immunity by tissue-resident
642 memory T (TRM) cells in the absence of persisting local antigen presentation.
643 *Proceedings of the National Academy of Sciences of the United States of America*
644 109:7037-7042.

645 Mackay, L.K., E. Wynne-Jones, D. Freestone, D.G. Pellicci, L.A. Mielke, D.M. Newman, A.
646 Braun, F. Masson, A. Kallies, G.T. Belz, and F.R. Carbone. 2015. T-box Transcription
647 Factors Combine with the Cytokines TGF-beta and IL-15 to Control Tissue-Resident
648 Memory T Cell Fate. *Immunity* 43:1101-1111.
649 Masopust, D., D. Choo, V. Vezys, E.J. Wherry, J. Duraiswamy, R. Akondy, J. Wang, K.A.
650 Casey, D.L. Barber, K.S. Kawamura, K.A. Fraser, R.J. Webby, V. Brinkmann, E.C.
651 Butcher, K.A. Newell, and R. Ahmed. 2010. Dynamic T cell migration program provides
652 resident memory within intestinal epithelium. *J Exp Med* 207:553-564.
653 Masopust, D., and A.G. Soerens. 2019. Tissue-Resident T Cells and Other Resident
654 Leukocytes. *Annu Rev Immunol* 37:521-546.
655 Masopust, D., V. Vezys, A.L. Marzo, and L. Lefrancois. 2001. Preferential localization of effector
656 memory cells in nonlymphoid tissue. *Science* 291:2413-2417.
657 Masopust, D., V. Vezys, E.J. Usherwood, L.S. Cauley, S. Olson, A.L. Marzo, R.L. Ward, D.L.
658 Woodland, and L. Lefrancois. 2004. Activated primary and memory CD8 T cells migrate
659 to nonlymphoid tissues regardless of site of activation or tissue of origin. *Journal of*
660 *immunology (Baltimore, Md. : 1950)* 172:4875-4882.
661 Masopust, D., V. Vezys, E.J. Wherry, D.L. Barber, and R. Ahmed. 2006. Cutting edge: gut
662 microenvironment promotes differentiation of a unique memory CD8 T cell population.
663 *Journal of immunology (Baltimore, Md. : 1950)* 176:2079-2083.
664 McKinnon, L.R., S.M. Hughes, S.C. De Rosa, J.A. Martinson, J. Plants, K.E. Brady, P.P. Gumbi,
665 D.J. Adams, L. Vojtech, C.G. Galloway, M. Fialkow, G. Lentz, D. Gao, Z. Shu, B.
666 Nyanga, P. Izulla, J. Kimani, S. Kimwaki, A. Bere, Z. Moodie, A.L. Landay, J.A.
667 Passmore, R. Kaul, R.M. Novak, M.J. McElrath, and F. Hladik. 2014. Optimizing viable
668 leukocyte sampling from the female genital tract for clinical trials: an international multi-
669 site study. *PLoS One* 9:e85675.

670 Milligan, G.N., D.I. Bernstein, and N. Bourne. 1998. T lymphocytes are required for protection of
671 the vaginal mucosae and sensory ganglia of immune mice against reinfection with
672 herpes simplex virus type 2. *Journal of immunology (Baltimore, Md. : 1950)* 160:6093-
673 6100.
674 Milner, J.J., C. Toma, B. Yu, K. Zhang, K. Omilusik, A.T. Phan, D. Wang, A.J. Getzler, T.
675 Nguyen, S. Crotty, W. Wang, M.E. Pipkin, and A.W. Goldrath. 2017. Runx3 programs
676 CD8(+) T cell residency in non-lymphoid tissues and tumours. *Nature* 552:253-257.
677 Morrison, L.A., X.J. Da Costa, and D.M. Knipe. 1998. Influence of mucosal and parenteral
678 immunization with a replication-defective mutant of HSV-2 on immune responses and
679 protection from genital challenge. *Virology* 243:178-187.
680 Park, S.L., A. Zaid, J.L. Hor, S.N. Christo, J.E. Prier, B. Davies, Y.O. Alexandre, J.L. Gregory,
681 T.A. Russell, T. Gebhardt, F.R. Carbone, D.C. Tscharke, W.R. Heath, S.N. Mueller, and
682 L.K. Mackay. 2018. Local proliferation maintains a stable pool of tissue-resident memory
683 T cells after antiviral recall responses. *Nature immunology* 19:183-191.
684 Parr, M.B., L. Kepple, M.R. McDermott, M.D. Drew, J.J. Bozzola, and E.L. Parr. 1994. A mouse
685 model for studies of mucosal immunity to vaginal infection by herpes simplex virus type
686 2. *Laboratory investigation; a journal of technical methods and pathology* 70:369-380.
687 Pattacini, L., A. Woodward Davis, J. Czartoski, F. Mair, S. Presnell, S.M. Hughes, O. Hyrien,
688 G.M. Lentz, A.C. Kirby, M.F. Fialkow, F. Hladik, M. Prlic, and J.M. Lund. 2019. A pro-
689 inflammatory CD8+ T-cell subset patrols the cervicovaginal tract. *Mucosal immunology*
690 Peng, T., J. Zhu, K. Phasouk, D.M. Koelle, A. Wald, and L. Corey. 2012. An effector phenotype
691 of CD8+ T cells at the junction epithelium during clinical quiescence of herpes simplex
692 virus 2 infection. *J Virol* 86:10587-10596.
693 Petro, C.D., B. Weinrick, N. Khajoueinejad, C. Burn, R. Sellers, W.R. Jacobs, Jr., and B.C.
694 Herold. 2016. HSV-2 DeltagD elicits FcgammaR-effector antibodies that protect against
695 clinical isolates. *JCI insight* 1:

696 Piet, B., G.J. de Bree, B.S. Smids-Dierdorp, C.M. van der Loos, E.B. Remmerswaal, J.H. von
697 der Thusen, J.M. van Haarst, J.P. Eerenberg, A. ten Brinke, W. van der Bij, W. Timens,
698 R.A. van Lier, and R.E. Jonkers. 2011. CD8(+) T cells with an intraepithelial phenotype
699 upregulate cytotoxic function upon influenza infection in human lung. *J Clin Invest*
700 121:2254-2263.
701 Pope, C., S.K. Kim, A. Marzo, D. Masopust, K. Williams, J. Jiang, H. Shen, and L. Lefrancois.
702 2001. Organ-specific regulation of the CD8 T cell response to Listeria monocytogenes
703 infection. *Journal of immunology (Baltimore, Md. : 1950)* 166:3402-3409.
704 Prlic, M., and M.J. Bevan. 2011. Cutting edge: beta-catenin is dispensable for T cell effector
705 differentiation, memory formation, and recall responses. *Journal of immunology*
706 *(Baltimore, Md. : 1950)* 187:1542-1546.
707 Prlic, M., B.R. Blazar, A. Khoruts, T. Zell, and S.C. Jameson. 2001. Homeostatic expansion
708 occurs independently of costimulatory signals. *Journal of immunology (Baltimore, Md. :*
709 *1950)* 167:5664-5668.
710 Reinhardt, R.L., A. Khoruts, R. Merica, T. Zell, and M.K. Jenkins. 2001. Visualizing the
711 generation of memory CD4 T cells in the whole body. *Nature* 410:101-105.
712 Schenkel, J.M., K.A. Fraser, V. Vezys, and D. Masopust. 2013. Sensing and alarm function of
713 resident memory CD8(+) T cells. *Nature immunology* 14:509-513.
714 Schiffer, J.T., L. Abu-Raddad, K.E. Mark, J. Zhu, S. Selke, D.M. Koelle, A. Wald, and L. Corey.
715 2010. Mucosal host immune response predicts the severity and duration of herpes
716 simplex virus-2 genital tract shedding episodes. *Proceedings of the National Academy of*
717 *Sciences of the United States of America* 107:18973-18978.
718 Schiffer, J.T., D. Swan, R. Al Sallaq, A. Magaret, C. Johnston, K.E. Mark, S. Selke, N.
719 Ocbamichael, S. Kuntz, J. Zhu, B. Robinson, M.L. Huang, K.R. Jerome, A. Wald, and L.
720 Corey. 2013. Rapid localized spread and immunologic containment define Herpes
721 simplex virus-2 reactivation in the human genital tract. *Elife* 2:e00288.

722 Shin, H., and A. Iwasaki. 2012. A vaccine strategy that protects against genital herpes by
723 establishing local memory T cells. *Nature* 491:463-467.
724 Steinbach, K., I. Vincenti, M. Kreutzfeldt, N. Page, A. Muschaweckh, I. Wagner, I. Drexler, D.
725 Pinschewer, T. Korn, and D. Merkler. 2016. Brain-resident memory T cells represent an
726 autonomous cytotoxic barrier to viral infection. *J Exp Med* 213:1571-1587.
727 Steinert, E.M., J.M. Schenkel, K.A. Fraser, L.K. Beura, L.S. Manlove, B.Z. Igyarto, P.J.
728 Southern, and D. Masopust. 2015. Quantifying Memory CD8 T Cells Reveals
729 Regionalization of Immunosurveillance. *Cell* 161:737-749.
730 Stephenson, K.E., H.T. D'Couto, and D.H. Barouch. 2016. New concepts in HIV-1 vaccine
731 development. *Curr Opin Immunol* 41:39-46.
732 Streeck, H. 2016. Designing optimal HIV-vaccine T-cell responses. *Curr Opin HIV AIDS* 11:593-
733 600.
734 Szabo, P.A., M. Miron, and D.L. Farber. 2019. Location, location, location: Tissue resident
735 memory T cells in mice and humans. *Sci Immunol* 4:
736 Takamura, S., H. Yagi, Y. Hakata, C. Motozono, S.R. McMaster, T. Masumoto, M. Fujisawa, T.
737 Chikaishi, J. Komeda, J. Itoh, M. Umemura, A. Kyusai, M. Tomura, T. Nakayama, D.L.
738 Woodland, J.E. Kohlmeier, and M. Miyazawa. 2016. Specific niches for lung-resident
739 memory CD8+ T cells at the site of tissue regeneration enable CD69-independent
740 maintenance. *J Exp Med* 213:3057-3073.
741 Tiemessen, M.M., M.R. Baert, L. Kok, M.C. van Eggermond, P.J. van den Elsen, R. Arens, and
742 F.J. Staal. 2014. T Cell factor 1 represses CD8+ effector T cell formation and function.
743 *Journal of immunology (Baltimore, Md. : 1950)* 193:5480-5487.
744 Wakim, L.M., J. Waithman, N. van Rooijen, W.R. Heath, and F.R. Carbone. 2008. Dendritic cell-
745 induced memory T cell activation in nonlymphoid tissues. *Science* 319:198-202.
746 Walsh, D.A., H. Borges da Silva, L.K. Beura, C. Peng, S.E. Hamilton, D. Masopust, and S.C.
747 Jameson. 2019. The Functional Requirement for CD69 in Establishment of Resident

Memory CD8(+) T Cells Varies with Tissue Location. *Journal of immunology (Baltimore, Md. : 1950)* 203:946-955.

Watanabe, R., A. Gehad, C. Yang, L.L. Scott, J.E. Teague, C. Schlapbach, C.P. Elco, V. Huang, T.R. Matos, T.S. Kupper, and R.A. Clark. 2015. Human skin is protected by four functionally and phenotypically discrete populations of resident and recirculating memory T cells. *Sci Transl Med* 7:279ra239.

Wu, J., A. Madi, A. Mieg, A. Hotz-Wagenblatt, N. Weisshaar, S. Ma, K. Mohr, T. Schlimbach, M. Hering, H. Borgers, and G. Cui. 2020. T Cell Factor 1 Suppresses CD103+ Lung Tissue-Resident Memory T Cell Development. *Cell Rep* 31:107484.

Zehn, D., S.Y. Lee, and M.J. Bevan. 2009. Complete but curtailed T-cell response to very low-affinity antigen. *Nature* 458:211-214.

Zhang, N., and M.J. Bevan. 2013. Transforming growth factor-beta signaling controls the formation and maintenance of gut-resident memory T cells by regulating migration and retention. *Immunity* 39:687-696.

Zhou, X., S. Yu, D.M. Zhao, J.T. Harty, V.P. Badovinac, and H.H. Xue. 2010. Differentiation and persistence of memory CD8(+) T cells depend on T cell factor 1. *Immunity* 33:229-240.

Zhu, J., D.M. Koelle, J. Cao, J. Vazquez, M.L. Huang, F. Hladik, A. Wald, and L. Corey. 2007. Virus-specific CD8+ T cells accumulate near sensory nerve endings in genital skin during subclinical HSV-2 reactivation. *J Exp Med* 204:595-603.

Zhu, J., T. Peng, C. Johnston, K. Phasouk, A.S. Kask, A. Klock, L. Jin, K. Diem, D.M. Koelle, A. Wald, H. Robins, and L. Corey. 2013. Immune surveillance by CD8alphaalpha+ skin-resident T cells in human herpes virus infection. *Nature* 497:494-497.

771 **Figure Legends**

772 **Figure 1. Human cervicovaginal-resident CD8 T cells lack expression of TCF-1. (A)** Gating
773 strategy to identify memory CD8 T cells in blood and CVT from healthy STI and HSV-2-negative
774 women. **(B)** Relative abundance of CD69 and CD103 subsets in blood and CVT. **(C)**
775 Representative flow plot and abundance of granzyme B^+ cells within the memory CD8
776 population in blood and CVT. **(D)** Representative flow plot and abundance of CD103 and
777 granzyme B co-expression in blood and CVT. **(E)** Representative TCF-1 staining and TCF-1^+
778 frequency from $CD103^+$ subset of CD8 T cells from the CVT compared to memory CD8 T cells
779 in matched blood. Flow plots from A and C-E are from one representative participant. Data from
780 B-E represent pooled results from study participants (n=13). Each dot in C-E represents an
781 individual participant. Error bars represent mean ± SD. *P*-value in E was calculated via paired *t*-
782 test. Exact *P*-values are given for all comparisons.

783

784 **Figure 2. Mouse cervicovaginal-resident CD8 T cells induced by vaginal immunization**
785 **mirror the phenotype observed in human samples and lack TCF-1. (A)** Experiment
786 schematic to induce CVT-resident CD8 T cells in mice via vaginal infection with 1.88×10^5 PFU
787 of thymidine kinase-negative HSV-2 186 kpn. **(B)** HSV-specific cells were identified in CVT via
788 staining with an H-2Kb SSIEFARL tetramer conjugated to APC. Left, representative flow plots
789 gated on CD8 T cells. Right, relative abundance of CD69 and CD103 subsets within gB
790 tetramer$^+$ CD8 T cells in CVT. **(C)** Representative flow plot and abundance of granzyme B^+ cells
791 within gB tetramer$^+$ CD8 T cells in CVT and CVT-draining lymph nodes (dLN). **(D)**
792 Representative TCF-1 staining and TCF-1^+ frequency within gB tetramer$^+$ CD8 T cells in CVT
793 and dLN. **(E)** Representative images of hematoxylin and eosin-stained sections of CVT at 10X
794 objective and average lamina propria inflammation scores. Arrow indicates coalescing clusters
795 of inflammatory cells with follicular organization. Arrowhead indicates clusters of inflammatory
796 cells within the mucosal epithelium. Flow plots and images from B-E are from one

797 representative mouse. Data from B-D represent pooled results from 2 independent experiments.
798 Each dot in E represents inflammation score averaged from 1-3 mice per time point. Error bars
799 represent mean ± SD. *P*-value in C was calculated via paired *t*-test. Exact *P*-values are given for
800 all comparisons.
801
802 **Figure 3. The cervicovaginal CD8 T cell memory compartment of LM-gB-immunized mice**
803 **is poorly maintained after immunization. (A)** Schematic of experiment to assess phenotype
804 and maintenance of HSV-specific T cell compartment of mice immunized with 4000 CFU LM-gB
805 i.v. **(B)** Representative image of hematoxylin and eosin-stained sections of CVT at 10X
806 objective and average lamina propria inflammation scores. **(C)** Representative flow plot gated
807 on CD8 T cells from blood collected 1wk after LM-gB immunization. **(D)** gB tetramer^{+} CD8 T cell
808 abundance in spleen, dLN, and CVT 1mo after immunization. **(E)** Representative TCF-1 staining
809 and quantification of TCF-1 expression within CD103^{+} and CD103^{-} subsets of gB tetramer^{+} CD8
810 T cells in CVT and dLN. **(F-G)** Relative abundance or number of HSV-specific CD8 T cells in
811 blood, spleen, dLN, small intestine lamina propria (SI LP), and CVT 1mo and 5mo after LM-gB
812 immunization. Images and flow plots from B, C, and E are from one representative mouse. Data
813 in D-G are pooled from 2-5 independent experiments. Each dot in B represents inflammation
814 score averaged from 2-3 mice per time point. Each dot in F represents the mean value of 20
815 mice from a representative experiment. Each dot in D, E, and G represents an individual mouse.
816 Error bars represent mean ± SD. *P*-value in B was calculated via *t*-test. *P*-values in E were
817 calculated with repeated measures ANOVA with Greenhouse-Geisser correction. *P*-values in G
818 were calculated via *t*-test using $\log_{10}$-transformed values. Exact *P*-values are given for all values
819 < 0.05.
820

821 **Figure 4. Most HSV-specific CD8 T cells remaining in the CVT by five months after**
822 **immunization express CD69 and CD103. (A)** Percentage of i.v. label$^-$ HSV-specific CD8 T
823 cells in different lymphoid and non-lymphoid tissues at 1mo, 3mo, and 5mo after immunization
824 based on gating shown in Fig. S1C. **(B)** Representative staining showing CD69 and CD103
825 expression on HSV-specific CD8 T cells in the CVT 1mo and 5mo after immunization. **(C)**
826 Stacked bar plots showing relative abundance of each of four subsets of HSV-specific CD8 T
827 cells based on CD69 and CD103 expression in the i.v. label$^+$ and i.v. label$^-$ fractions of the CVT
828 and SI LP. **(D)** CD103 expression on i.v. label$^-$ gB tetramer$^+$ CD8 T cells in the CVT 1mo, 3mo,
829 and 5mo after immunization. **(E)** Total i.v. label$^-$ count of each of four subsets of HSV-specific
830 CD8 T cells based on CD69 and CD103 expression 1mo, 3mo, and 5mo after immunization.
831 Data in A, C, D, and E are pooled from at least 2 independent experiments per time point. Data
832 in B are from one representative experiment. Each dot in A, D, and E represents an individual
833 mouse. Error bars represent mean ± SD. *P*-values in D and E were calculated via ordinary one-
834 way ANOVA with Tukey's post-hoc test using $\log_{10}$-transformed values for numbers and
835 untransformed values for percentages. Exact *P*-values are given for all values <0.05.
836
837 **Figure 5. After systemic immunization, cervicovaginal-resident CD8 T cells progressively**
838 **upregulate granzyme B. (A)** Frequency of granzyme B$^+$ cells among HSV-specific CD8 T cells
839 in spleen, dLN, CVT, and SI LP at 1mo, 3mo, and 5mo post-immunization. **(B)** Number of
840 granzyme B-expressing cells among HSV-specific CD8 T cells at time points after LM-gB
841 immunization. **(C)** Concatenated flow files from 10 mice showing CD103 and granzyme B co-
842 expression among the HSV-specific CD8b i.v. label$^-$ populations in the CVT and dLN 5mo after
843 LM-gB immunization. **(D-E)** Frequency of CD69 and CD103 expression within granzyme B$^+$
844 HSV-specific CD8 T cells in the CVT and SI LP 1mo, 3mo, and 5mo after immunization. Data in
845 A-E are pooled from at least 2 independent experiments. Each dot or triangle in A, B, and D
846 represents an individual mouse. Error bars represent mean ± SD. *P*-values in A and B were

847 calculated via ordinary one-way ANOVA with Tukey's post-hoc test using $\log_{10}$-transformed
848 values for numbers and untransformed values for percentages. Exact *P*-values are given for all
849 values <0.05.
850
851 **Figure 6. LM-gB immunized mice are protected against severe disease after lethal**
852 **intravaginal challenge with HSV-2, but the efficacy of the immune response wanes over**
853 **time. (A)** Experiment schematic to compare protective efficacy of LM-gB immunization 1mo and
854 4mo after administration. **(B)** Survival after vaginal HSV-2 challenge of naive and LM-gB
855 immunized mice. **(C)** Vaginal washes were collected after HSV-2 challenge and HSV-2 titer was
856 determined by plaque assay. Pink dots represent mice that survived challenge, as shown in B.
857 **(D)** Number of HSV-specific CD8 T cells (top) and HSV genomes (bottom) in the CVT with
858 modeling estimates overlaid in blue. **(E)** Schematic of mathematical model relating CVT-
859 infiltrating CD8 T cell immune response to HSV-2 viral expansion kinetics. *S* and *I* represent the
860 number of susceptible and infected cells per CVT, respectively; *E*, the number of gB tet^+ CD8 T
861 cells per CVT; and *V* the number of HSV genomes per vaginal wash. **(F)** Model estimates of
862 basic reproductive ratios (number of new cells infected by one infected cell when introduced into
863 a pool of susceptible cells) for each group of mice. **(G)** Scatter plot of areas under curves (AUC)
864 from D and corresponding predicted day of viral clearance. Dotted line represents a fitted line
865 from quadratic regression. Data in B, C, and D are pooled from at least 2 independent
866 experiments (n=8-14 per group in B). Each dot, square, or triangle in B, C, and D represents
867 data from an individual mouse. Each dot, square, or triangle in F and G represents one model
868 estimate. Error bars in C represent mean ± SD. *P*-values in C were calculated via unpaired *t*-
869 test using $\log_{10}$-transformed values. *P*-values in F were calculated via pairwise-corrected Mann-
870 Whitney's test using Bonferroni's correction. *P*- and r_s-value in G were calculated via
871 Spearman's rank correlation. Exact *P*-values are given for all values <0.05.
872

873 **Figure 7. Differentiation and decay of the CVT-resident CD8 T cell compartment is tissue-**
874 **intrinsic (A)** Schematic of experiment to test effect of depleting circulating gBT-I cells. **(B)**
875 Example flow staining to identify gBT-I population within CD8 T cells from spleen and CVT of
876 depleted or undepleted mice 1mo after immunization. **(C)** Number of gBT-I cells recovered from
877 spleen or CVT of mice at indicated time points after immunization. **(D-E)** Relative abundance of
878 CD69 and CD103 subsets within i.v. label^{-} gBT-I cells in CVT at indicated time points. **(F)**
879 Frequency of granzyme B expression among gBT-I cells. **(G)** Frequency of TCF-1 expression
880 among i.v. label^{-} gBT-I cells. Data in C-G are pooled from 2 independent experiments. Flow
881 plots in B are derived from two representative mice. Each dot in C, E, F, and G represents an
882 individual mouse. Error bars represent mean ± SD. *P*-values in C, E, and F were calculated via
883 unpaired *t*-test comparing 1mo to 3mo within each depletion group. *P*-values in G were
884 calculated via ordinary one-way ANOVA with Tukey's post-hoc test. Exact *P*-values are given
885 for all values <0.05.
886
887 **Figure 8. Decay of the CVT-resident CD8 T cell compartment occurs regardless of**
888 **priming infection and route. (A)** Schematic of experiment to assess effect of vaginal
889 immunization on longevity of memory CD8 T cells in CVT. **(B)** Number of gB tetramer^{+} cells
890 recovered from spleen, SI LP, or CVT of mice at indicated time points after immunization. Each
891 dot in B represents an individual mouse. Error bars represent mean ± SD. *P*-values in B were
892 calculated via unpaired *t*-test comparing 1mo to 3mo within each immunization group. Exact *P*-
893 values are given for all values <0.05.
894
895

Figure 1

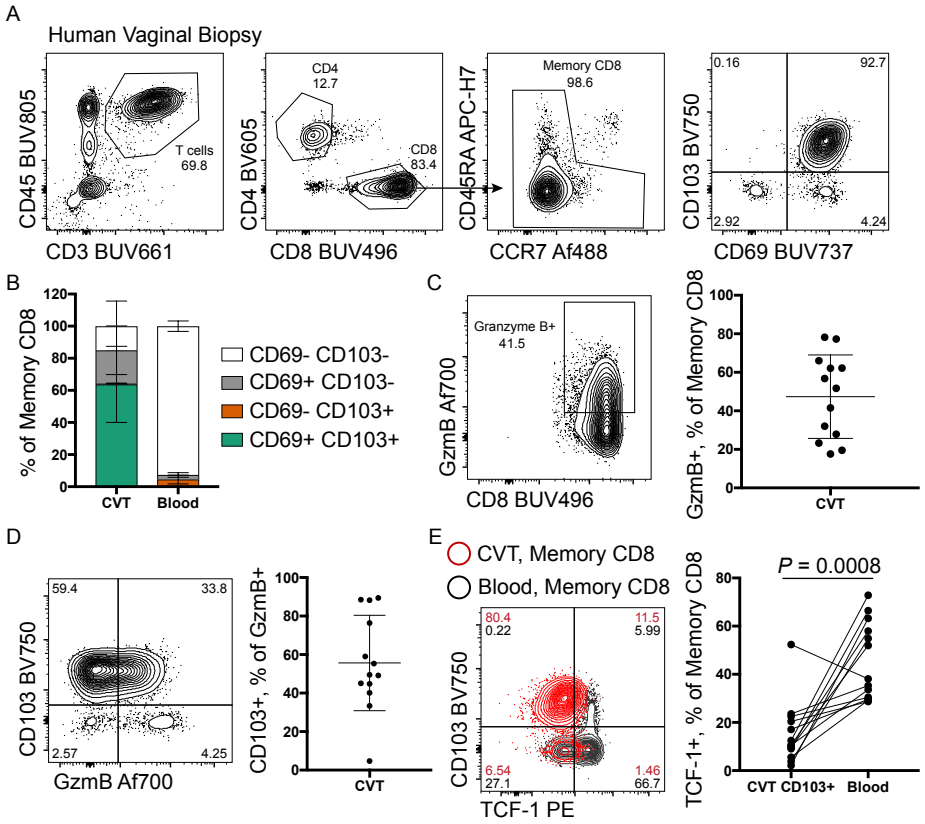
A
Human Vaginal Biopsy
CD45 BUV805
CD3 BUV661
T cells
69.8
CD4 BV605
CD8 BUV496
CD4
12.7
CD8
83.4
CD45RA APC-H7
CCR7 Af488
Memory CD8
98.6
CD103 BV750
CD69 BUV737
0.16
92.7
2.92
4.24
B
% of Memory CD8
CVT
Blood
CD69- CD103-
CD69+ CD103-
CD69- CD103+
CD69+ CD103+
C
GzmB Af700
CD8 BUV496
Granzyme B+
41.5
GzmB+, % of Memory CD8
CVT
D
CD103 BV750
GzmB Af700
59.4
33.8
2.57
4.25
CD103+, % of GzmB+
CVT
E
CVT, Memory CD8
Blood, Memory CD8
CD103 BV750
TCF-1 PE
80.4
0.22
11.5
5.99
6.54
27.1
1.46
66.7
TCF-1+, % of Memory CD8
P = 0.0008
CVT CD103+
Blood

Figure 2

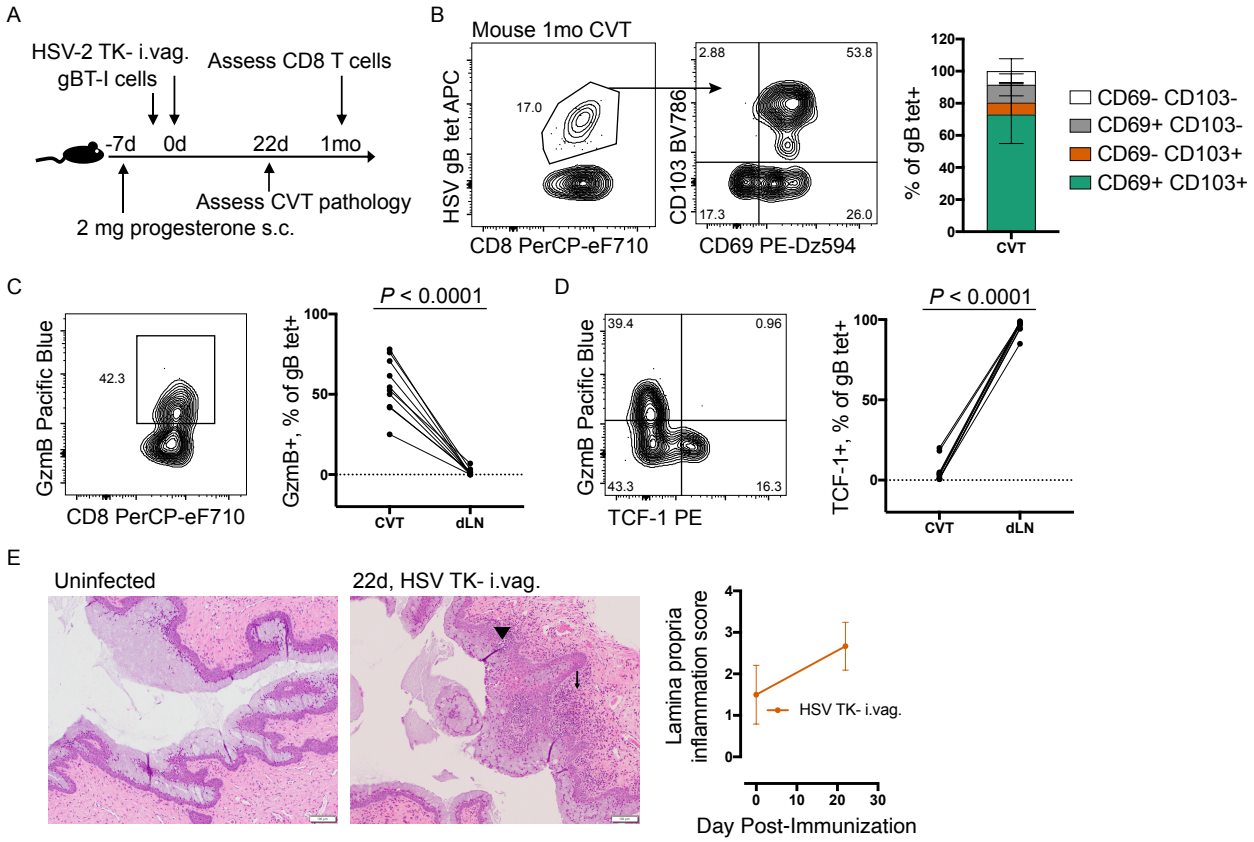
A
HSV-2 TK- i.vag.
gBT-I cells
Assess CD8 T cells
-7d
0d
22d
1mo
Assess CVT pathology
2 mg progesterone s.c.
B
Mouse 1mo CVT
HSV gB tet APC
17.0
CD8 PerCP-eF710
CD103 BV786
2.88
53.8
17.3
26.0
CD69 PE-Dz594
% of gB tet+
CVT
CD69- CD103-
CD69+ CD103-
CD69- CD103+
CD69+ CD103+
C
GzmB Pacific Blue
42.3
CD8 PerCP-eF710
GzmB+, % of gB tet+
P < 0.0001
CVT
dLN
D
GzmB Pacific Blue
39.4
0.96
43.3
16.3
TCF-1 PE
TCF-1+, % of gB tet+
P < 0.0001
CVT
dLN
E
Uninfected
22d, HSV TK- i.vag.
Lamina propria inflammation score
HSV TK- i.vag.
Day Post-Immunization

Figure 3

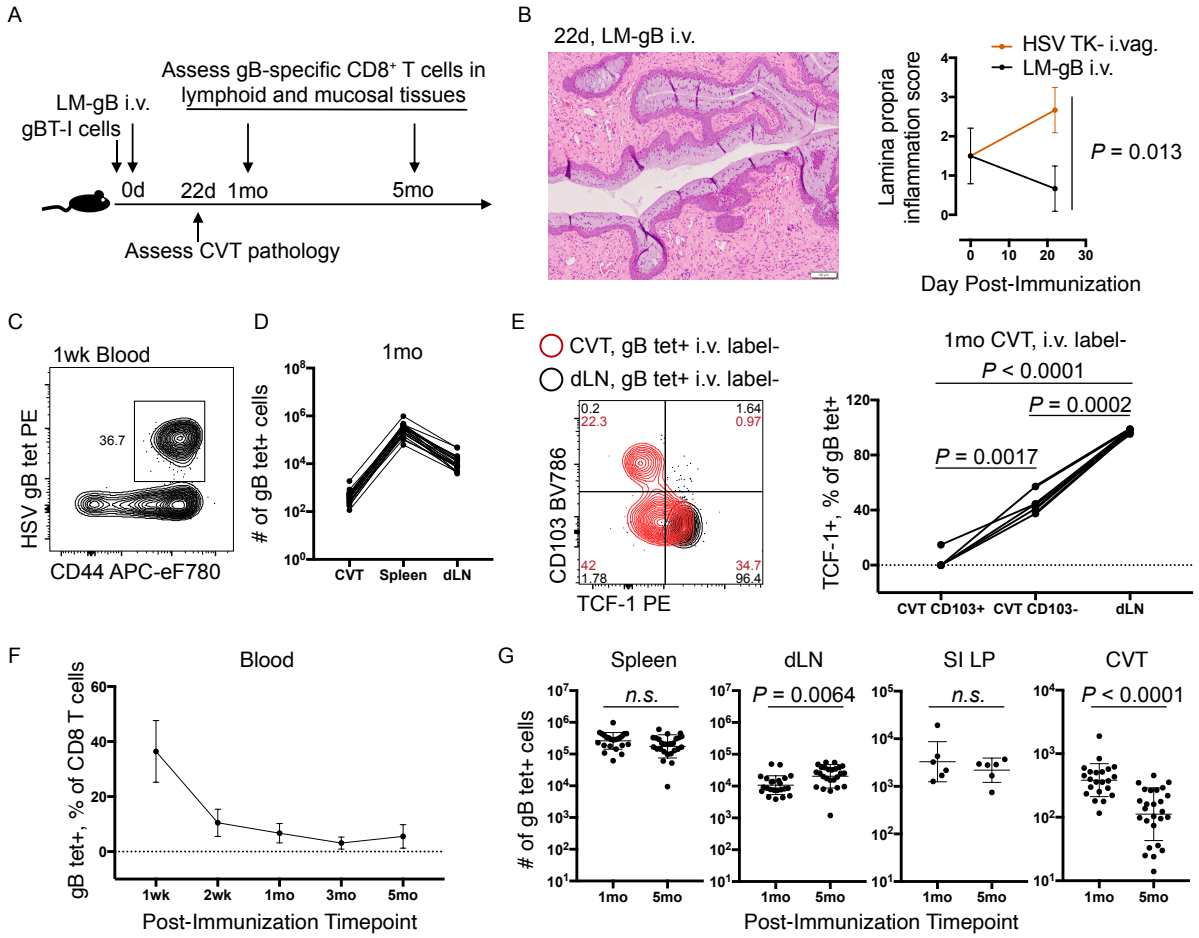
A
Assess gB-specific CD8+ T cells in lymphoid and mucosal tissues
LM-gB i.v.
gBT-I cells
0d
22d
1mo
5mo
Assess CVT pathology
B
22d, LM-gB i.v.
HSV TK- i.vag.
LM-gB i.v.
Lamina propria inflammation score
P = 0.013
Day Post-Immunization
C
1wk Blood
36.7
HSV gB tet PE
CD44 APC-eF780
D
1mo
# of gB tet+ cells
CVT
Spleen
dLN
E
CVT, gB tet+ i.v. label-
dLN, gB tet+ i.v. label-
CD103 BV786
TCF-1 PE
1mo CVT, i.v. label-
P < 0.0001
P = 0.0002
P = 0.0017
TCF-1+, % of gB tet+
CVT CD103+
CVT CD103-
dLN
F
Blood
gB tet+, % of CD8 T cells
1wk
2wk
1mo
3mo
5mo
Post-Immunization Timepoint
G
Spleen
dLN
SI LP
CVT
n.s.
P = 0.0064
n.s.
P < 0.0001
# of gB tet+ cells
1mo
5mo
Post-Immunization Timepoint

Figure 4

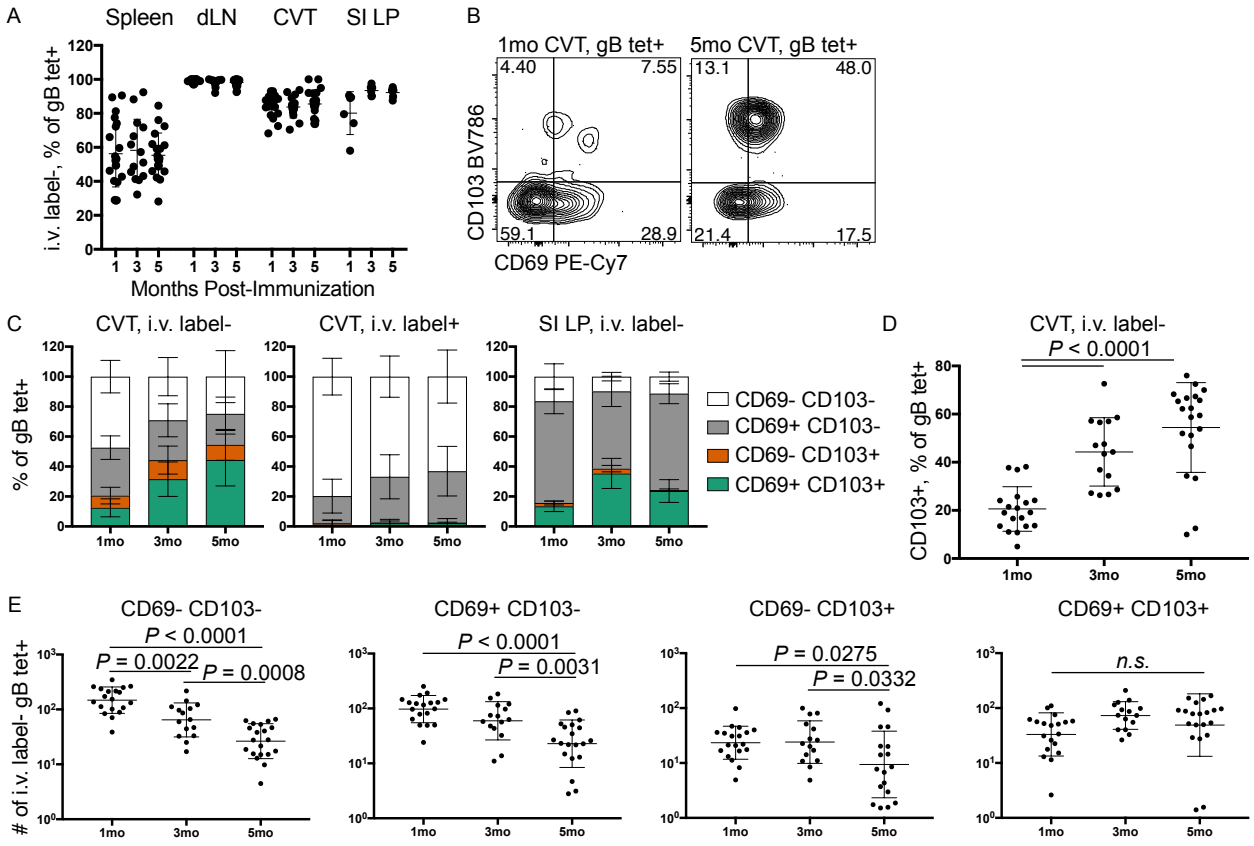
A
Spleen
dLN
CVT
SI LP
i.v. label-, % of gB tet+
Months Post-Immunization
B
1mo CVT, gB tet+
5mo CVT, gB tet+
4.40
7.55
59.1
28.9
13.1
48.0
21.4
17.5
CD103 BV786
CD69 PE-Cy7
C
CVT, i.v. label-
CVT, i.v. label+
SI LP, i.v. label-
% of gB tet+
1mo
3mo
5mo
CD69- CD103-
CD69+ CD103-
CD69- CD103+
CD69+ CD103+
D
CVT, i.v. label-
P < 0.0001
CD103+, % of gB tet+
E
CD69- CD103-
P < 0.0001
P = 0.0022
P = 0.0008
CD69+ CD103-
P < 0.0001
P = 0.0031
CD69- CD103+
P = 0.0275
P = 0.0332
CD69+ CD103+
n.s.
# of i.v. label- gB tet+

Figure 5

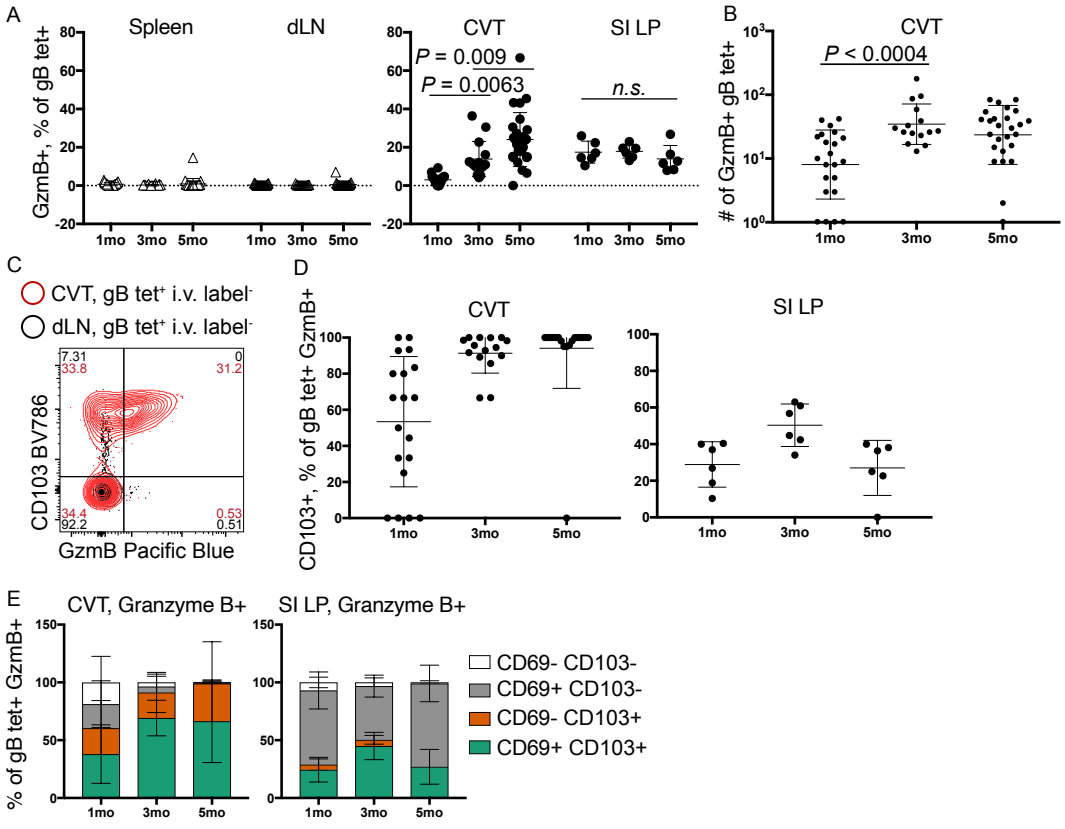
A
Spleen
dLN
CVT
SI LP
GzmB+, % of gB tet+
P = 0.009
P = 0.0063
n.s.
1mo 3mo 5mo
B
CVT
P < 0.0004
# of GzmB+ gB tet+
C
CVT, gB tet+ i.v. label-
dLN, gB tet+ i.v. label-
CD103 BV786
GzmB Pacific Blue
D
CVT
SI LP
CD103+, % of gB tet+ GzmB+
E
CVT, Granzyme B+
SI LP, Granzyme B+
% of gB tet+ GzmB+
CD69- CD103-
CD69+ CD103-
CD69- CD103+
CD69+ CD103+

Figure 6

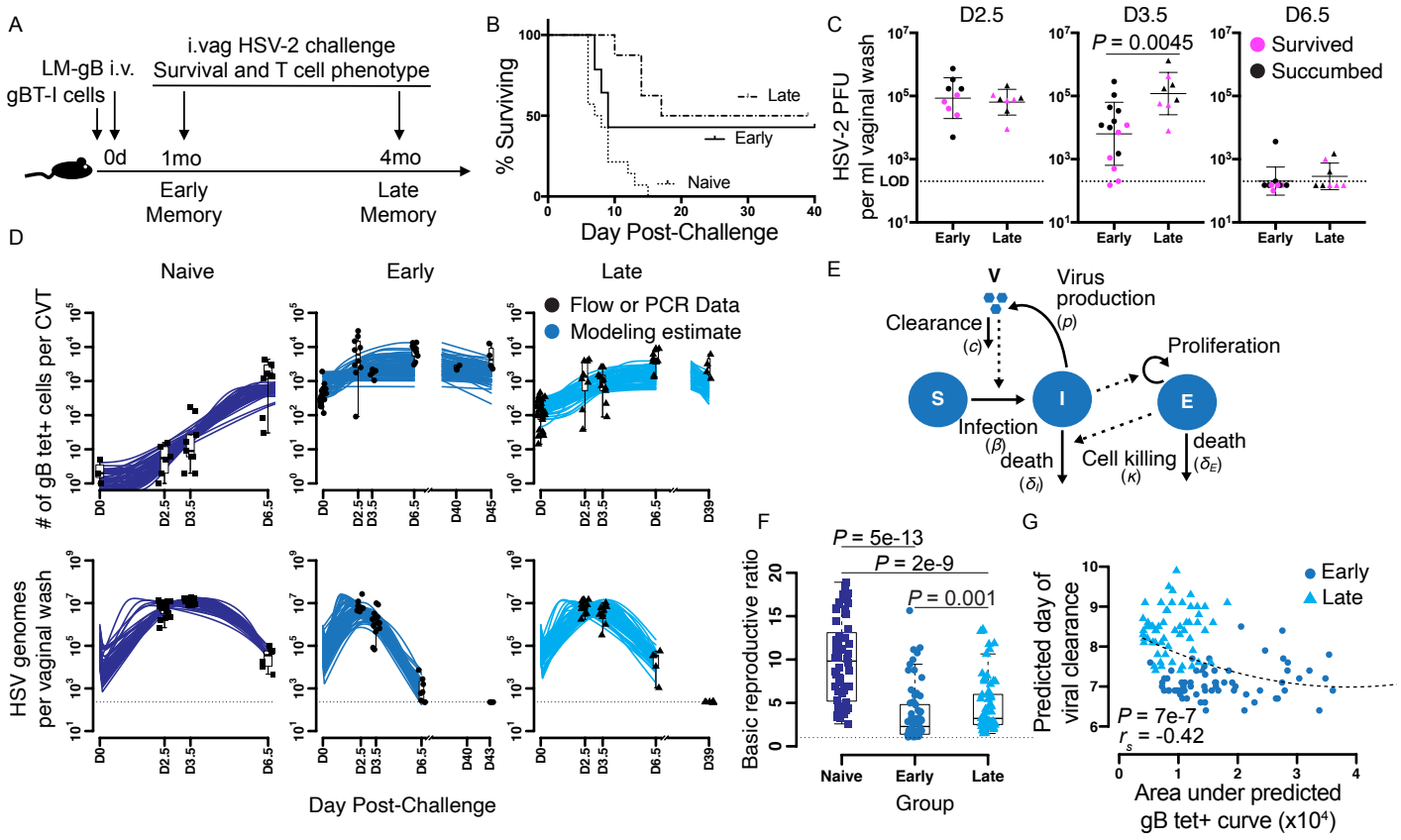
A
LM-gB i.v.
gBT-I cells
i.vag HSV-2 challenge
Survival and T cell phenotype
0d
1mo
4mo
Early Memory
Late Memory
B
% Surviving
Day Post-Challenge
Late
Early
Naive
C
HSV-2 PFU per ml vaginal wash
D2.5
D3.5
D6.5
P = 0.0045
Survived
Succumbed
LOD
Early
Late
D
Naive
Early
Late
Flow or PCR Data
Modeling estimate
# of gB tet+ cells per CVT
HSV genomes per vaginal wash
Day Post-Challenge
E
V
Virus production
(p)
Clearance
(c)
Proliferation
S
I
E
Infection
(β)
death
(δI)
Cell killing
(κ)
death
(δE)
F
Basic reproductive ratio
P = 5e-13
P = 2e-9
P = 0.001
Naive
Early
Late
Group
G
Predicted day of viral clearance
Early
Late
P = 7e-7
rs = -0.42
Area under predicted gB tet+ curve (x10⁴)

Figure 7

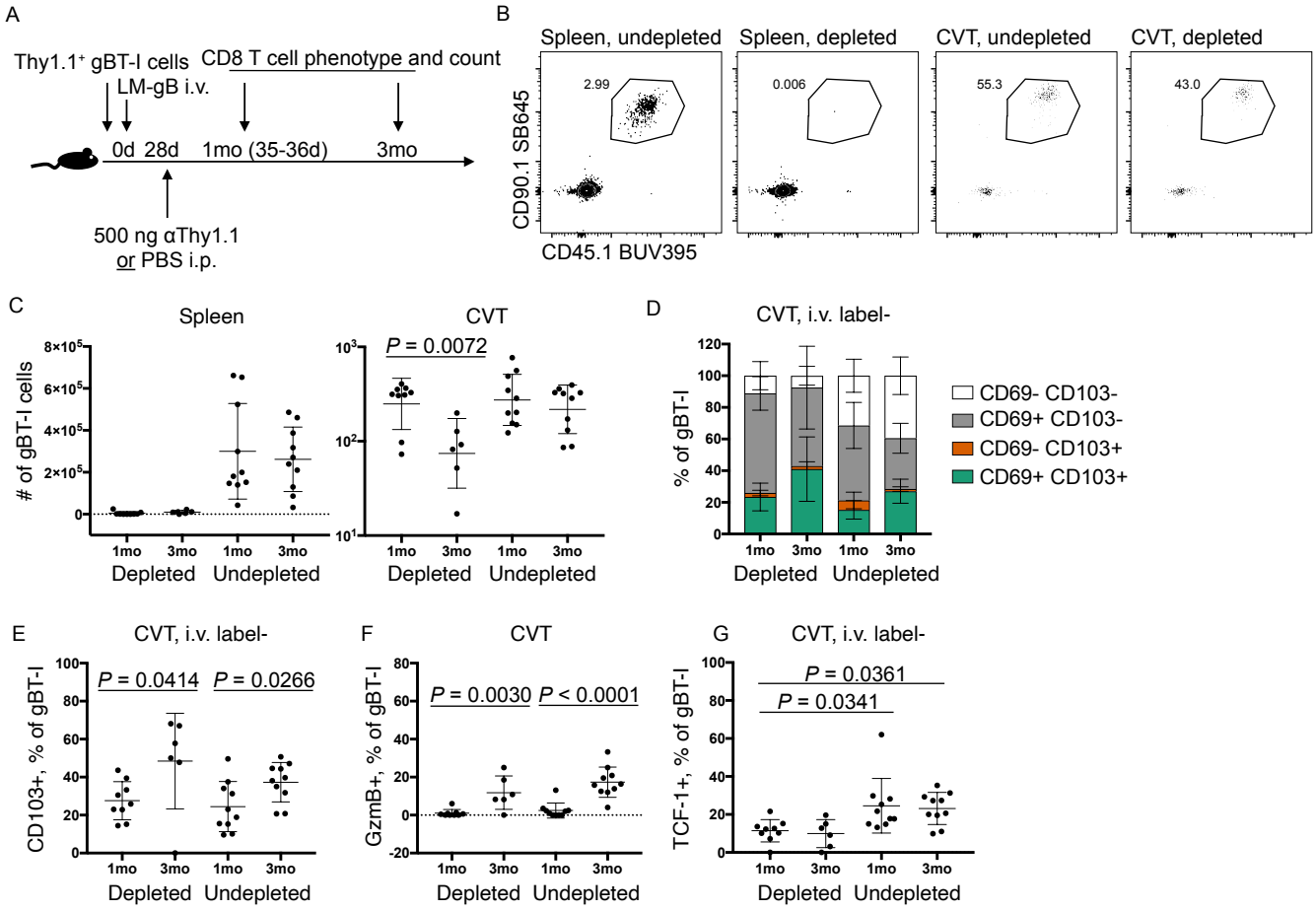
A
Thy1.1+ gBT-I cells
LM-gB i.v.
CD8 T cell phenotype and count
0d 28d 1mo (35-36d) 3mo
500 ng αThy1.1
or PBS i.p.
B
Spleen, undepleted
Spleen, depleted
CVT, undepleted
CVT, depleted
2.99
0.006
55.3
43.0
CD90.1 SB645
CD45.1 BUV395
C
Spleen
CVT
# of gBT-I cells
P = 0.0072
1mo 3mo 1mo 3mo
Depleted Undepleted
D
CVT, i.v. label-
% of gBT-I
CD69- CD103-
CD69+ CD103-
CD69- CD103+
CD69+ CD103+
E
CVT, i.v. label-
CD103+, % of gBT-I
P = 0.0414
P = 0.0266
F
CVT
GzmB+, % of gBT-I
P = 0.0030
P < 0.0001
G
CVT, i.v. label-
TCF-1+, % of gBT-I
P = 0.0361
P = 0.0341

Figure 8

A

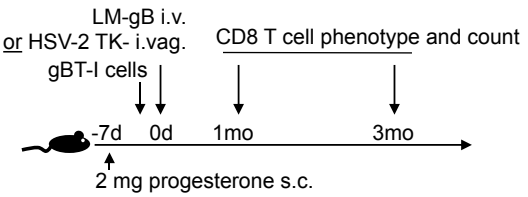
LM-gB i.v.
or HSV-2 TK- i.vag.
gBT-I cells
CD8 T cell phenotype and count
-7d
0d
1mo
3mo
2 mg progesterone s.c.

B

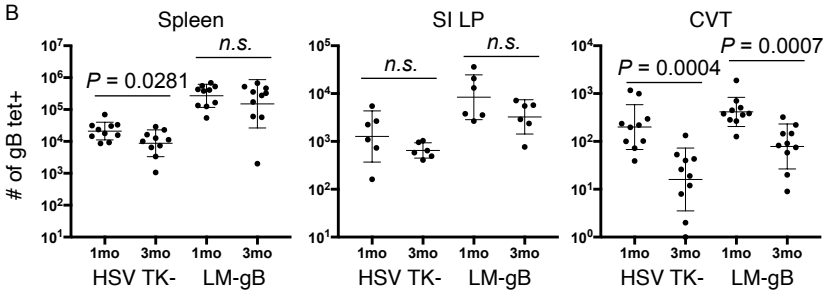
Spleen
SI LP
CVT
# of gB tet+
P = 0.0281
n.s.
n.s.
n.s.
P = 0.0004
P = 0.0007
1mo
3mo
1mo
3mo
HSV TK-
LM-gB